1 RESEARCH ARTICLE

2 Vernalization alters sugar beet (*Beta vulgaris*) sink and source
3 identities and reverses phloem translocation from taproots to shoots

4 **Cristina Martins Rodrigues[1*], Christina Müdsam[2*], Isabel Keller[1], Wolfgang Zierer[2], Olaf**
5 **Czarnecki[3], José María Corral[2], Frank Reinhardt[1], Petra Nieberl[4], Frederik Sommer[5],**
6 **Michael Schroda[5], Timo Mühlhaus[6], Karsten Harms[7], Ulf-Ingo Flügge[8], Uwe Sonnewald[2],**
7 **Wolfgang Koch[3], Frank Ludewig[3], H. Ekkehard Neuhaus[1], Benjamin Pommerrenig[1§]**

8 [1] Plant Physiology, University of Kaiserslautern, Kaiserslautern, Germany
9 [2] Biochemistry, FAU Erlangen-Nürnberg, Erlangen, Germany
10 [3] KWS SAAT SE & Co. KGaA, Einbeck, Germany
11 [4] Molecular Plant Physiology, FAU Erlangen-Nürnberg, Erlangen, Germany
12 [5] Biotechnology, University of Kaiserslautern, Kaiserslautern, Germany
13 [6] Bioinformatics, University of Kaiserslautern, Kaiserslautern, Germany
14 [7] Südzucker AG, CRDS, Obrigheim/Pfalz, Germany
15 [8] Botanical Institute, Cologne Biocenter and Center of Excellence on Plant Science (CEPLAS),
16 Cologne, Germany

17 [*]These authors contributed equally to this work, [§]corresponding author (pommerre@bio.uni-kl.de)

18 **Short title:** Sugar beet sink source reversion

19 **One-sentence summary:** Cold treatment transforms sugar beet (*Beta vulgaris*) taproots from
20 sucrose-storing sink organs to sucrose-mobilizing source organs prior to bolting.

24 ABSTRACT

25 During vegetative growth, biennial sugar beets maintain a steep gradient between the shoot (source)
26 and the sucrose-storing taproot (sink). To shift from vegetative to generative growth, they require
27 a chilling phase, called vernalization. Here, we studied sugar beet sink-source dynamics upon cold
28 temperature-induced vernalization and revealed a pre-flowering taproot sink to source reversal.
29 This transition is induced by transcriptomic and functional reprogramming of sugar beet tissue,
30 resulting in a reversal of flux direction in long distance transport system, the phloem. As a key
31 process for this transition, vacuolar sucrose importers and exporters, BvTST2;1 and BvSUT4, are
32 oppositely regulated, leading to re-mobilization of sugars from taproot storage vacuoles.
33 Concomitant changes in the expression of floral regulator genes suggest that the now deciphered
34 processes are a prerequisite for bolting. Our data may thus serve dissecting metabolic and
35 developmental triggers for bolting, which are potential targets for genome editing or breeding
36 approaches.

Funding

Introduction

Plants modulate not only the shape and size of their organs, but also physiological and molecular properties in these structures during development and as a response to environmental stimuli. In general, sink organs in plants depend on the import of carbohydrates, mainly sucrose, from source organs. However, previous sink organs may differentiate into 'sources', which then, in turn, provide mobilized storage products to newly emerging sinks.

The relative strengths of sinks and sources can be adjusted by the activity of sucrose synthesizing and degrading enzymes (Herbers and Sonnewald, 1998), and by alteration of the activities of phloem located sucrose loaders (Imlau et al., 1999; Gottwald et al., 2000; Srivastava et al., 2008; Chen et al., 2012). As a consequence, both, sucrose metabolizing enzymes and transporters represent targets relevant for breeding strategies aiming at yield increase of crops (Ludewig and Sonnewald, 2016; Sonnewald and Fernie, 2018).

Sucrose is the primary sugar transported in the phloem from source to sink organs. After unloading at the sinks, sucrose can be used as energy precursor, and as building block for growth and storage compound biosynthesis. Non-green storage organs like tubers or taproots must maintain a steep source to sink gradient. To do so, imported sucrose is rapidly converted into relatively inert storage compounds like starch or is compartmentalized intracellularly into large cell vacuoles. As given, sink and source identities of plant organs are dynamic and corresponding transitions are initiated after onset of endogenous developmental signals (Turgeon, 1989) or in response to specific environmental stimuli (Roitsch, 1999). Thus, dynamic regulation of genes and enzymes involved in carbohydrate metabolism and import of sugars into the phloem of mobilizing storage organs are key for source establishment of former sinks (Viola et al., 2007; Liu et al., 2015; O'Neill et al., 2013; Boussiengui-Boussiengui et al., 2016).

Sugar beet (*Beta vulgaris*), the major crop species providing industrial sucrose in the temperate zones of Europe and North America, exhibits a biennial lifecycle and forms a large taproot during the first year of its development. This taproot represents a reversible sink, which contains up to 20% of its fresh weight as sucrose. The vacuolar sucrose loader, named T̲ONOPLAST S̲UGAR

67   TRANSPORTER2;1 (*Bv*TST2;1), has been identified to be a key element for sugar accumulation

68   in this storage organ (Jung et al., 2015). During the second year the taproot provides previously

69   stored sucrose as precursor for the formation of a markedly large inflorescence.

70   The emergence of the sugar beet inflorescence strictly depends on a previous phase of cold

71   temperatures, which induces molecular reprogramming known as vernalization. This vernalization-

72   dependent bolting leads to significant loss of taproot sugar and biomass, and therefore yield. This

73   loss of yield contributes to the fact that sugar beets are solely cultivated as an annual crop.

74   Accordingly, sugar beet is sown in spring and harvested in the following late autumn. A prolonged

75   cultivation period (particularly autumn to autumn) and thus, identification of bolting-resistant

76   varieties have therefore become primary goals in sugar beet breeding over the last decades

77   (Hoffmann and Kluge-Severin, 2011; Hoffmann and Kenter, 2018).

78   Two major early-bolting loci, *B* and *B2* have been identified in the sugar beet genome in recent

79   years, encoding the pseudo response regulator gene *BOLTING TIME CONTROL 1*, *BTC1* (Pin et

80   al., 2012) and the *DOUBLE B-BOX TYPE ZINC FINGER* protein *BvBBX19* (Dally et al., 2014),

81   respectively. In annual beets, expression of both genes leads to repression of the floral repressor

82   gene *FT1*, and subsequent induction of the floral inducer gene *FT2* and vernalization-independent

83   flowering upon long-days (Pin et al., 2010; Dally et al., 2014). Biennial beets are homozygous for

84   the recessive *btc1* and *bbx19* alleles, which encode non-functional proteins unable to repress the

85   inhibitory function of FT1 (Pfeiffer et al., 2014). Accordingly, biennial sugar beets require

86   vernalization for BTC1- and BBX19-independent *FT1* repression and flowering (Pin et al., 2010).

87   Obviously, floral induction and sink-source transition must be tightly interconnected in sugar beet.

88   A coordinated network of floral inducers and repressors initiates the transition to bolting after

89   vernalization, but adjustment of the metabolic set-up appears equally important for the

90   morphological and physiological restructuring of taproots prior to formation of inflorescences.

91   However, little information is available on the molecular physiological processes in sugar beet at

92   the early time points of vernalization.

93   In this work, we therefore sought to understand how chilling temperatures, representing a *condition*

94   *sine qua non* for vernalization, might influence sugar metabolism, photosynthesis, phloem

95   translocation, and therefore source and sink identities of shoots and taproots. We combined

96   comprehensive transcriptome and proteome analyses with recording of organ growth

97   characteristics, photosynthetic parameters and metabolite quantification. In summary, our analyses

98   revealed an unexpected cold-dependent reversal of sink and source identities of taproots and shoots,

99   respectively, prior to bolting at the very early stages of vernalization.

100   Despite inactivation of photosynthesis in the cold, shoot biomass increased at the expense of

101   taproot sucrose. We recorded a substantial export of taproot sugar in the cold, which correlates

102   with altered activities of sugar ex- and importers and with a markedly altered expression of genes

103   involved in either sucrose synthesis or degradation. We speculate that this so far hidden metabolic

104   reprogramming is a prerequisite for initiation of bolting as corresponding flux redirection transports

105   sugars from the taproot to the shoot. However, this process might also contribute to the pronounced

106   frost sensitivity of sugar beet. Thus, our findings provide a molecular-physiological explanation to

107   the well-known problem of sugar beet cultivation (loss of yield due to the biennial lifecycle) and

108   provide new targets to achieve bolting resistance and winter hardiness in this crop species.

109   **Results**

110   **Cold exposure causes rapid loss of shoot and root water, but not of shoot biomass production**

111   To resolve cold-dependent growth dynamics of sugar beet source and sink organs, we monitored

112   shoot and taproot weights of plants from three different hybrid genotypes (GT1, GT2, and GT3),

113   (initially grown under control conditions [20°C], then acclimated for one week at 12°C) for 19 days

114   after transfer to cold (4°C) conditions (**Figure 1**). Shoot dry weight (DW), but not fresh weight

115   (FW) continued to increase during the exposure of the plants to 4°C. Consequently, shoot water

116   content gradually decreased by almost half at the end of the recorded time (**Figure 1A**).

117   Simultaneously, FW but also DW of taproots decreased together with the taproot water content

118   during the cold exposure period (**Figure 1A, B**). These results showed that growth of taproots was

119   more affected than that of shoots in the cold and suggested differential physiological and metabolic

120   responses of the shoot and root tissues to cold exposure.

121   **Sugar levels behave differently in shoots and taproots in the cold**

122   Accumulation of soluble sugars in shoots is a common response to low temperatures and part of

123   cold acclimation process of many plant species (Steponkus, 1971; Wolfe and Bryant, 1999; Strand

124   et al., 1997). Also, in our cold-dependent growth analysis, leaf material (obtained from the very

125   same sugar beet plants as was used for biomass and water content calculation (**Figure 1A**))

126   exhibited a clear increase in the levels of glucose and fructose (and to a lesser extent of the

127   disaccharide sucrose) after transfer to 4°C (**Figure 1C**). In contrast to soluble sugars, leaf starch

128   contents in all three genotypes decreased rapidly after transfer to 4°C, reaching 20 to 33% of the

129   value present prior to transfer (**Figure 1C, rightmost panel**).

130   In taproot tissue, sugar accumulation dynamics differed markedly from those in shoots. Glucose

131   and fructose levels slightly increased in the cold, but reached only between 10 to 20 percent of the

132   monosaccharide concentrations of leaves. Prior to transfer to 4°C, taproot sucrose levels exceeded

133   those of monosaccharides 30- to 100-fold. Taproot starch levels of all genotypes were extremely

134   low and did hardly change during cold treatment (**Figure 1D**). The three genotypes analyzed,

135   however, exhibited different sugar and starch accumulation dynamics in the cold. While GT2 and

136   GT3 taproot sucrose levels clearly decreased in the cold, GT1 sucrose levels fluctuated only

137   marginally. Interestingly, the steep drop in sucrose concentration in taproots of GT3 (by about 400

138   µmol/g DW) and to a lesser extend of GT2 (by about 200 µmol/g DW) was not accompanied by a

139   proportionate increase of monosaccharides, as would be expected for an exclusive hydrolysis of

140   sucrose. These massive losses of taproot sucrose rather suggested that this sugar was either (i)

141   increasingly respired, (ii) converted into compounds other than the monosaccharides glucose and

142   fructose, or (iii) exported from the taproot tissue into other organs. In the following, we aimed to

143   elucidate the fate of sucrose with respect to these possibilities.

144   **Cold exposure affects photosynthesis rate and carbon dioxide assimilation**

145   In cold tolerant plants like Arabidopsis, sugars accumulate in leaves in the cold when

146   photosynthetic activity is maintained during reduced sucrose phloem loading and increased sugar

147   import into vacuoles of leaf mesophyll cells (Strand et al., 1997; Wingenter et al., 2010;

148   Pommerrenig et al., 2018). We analyzed the impact of cold on sugar beet photosynthesis with pulse

149   amplitude modulated (PAM) fluorometry and CO_2 assimilation with gas exchange measurements

150   (**Figure 2**). These measurements revealed that Photosystem II quantum yield (Y(II)), leaf CO_2

151   concentrations (C_i), CO_2 assimilation rate (A), and leaf transpiration rate (E) were dependent on

152   the ambient temperature and that plants exposed to cold responded with a decline in photosynthetic

153   efficiency (**Figure 2**). All three genotypes showed a slight but significant reduction of Y(II) already

154   after one week transfer to 12°C. Simultaneously, non-photochemical quenching Y(NPQ) increased,

155   and non-regulated energy dissipation Y(NO) decreased at this temperature in the leaves of all three

156   genotypes (**Figure 2A**). The higher Y(NPQ) quantum yield at 12 °C compared to 20°C indicated

157   an increased flow of electrons towards the Mehler-Ascorbate peroxidase pathway (Asada et al.,

158   1998) upon exposure to this temperature to undergo e.g. thermal energy dissipation at Photosystem

159   II reaction centers. After transfer to 4°C, Y(II) decreased further and did not recover over the time

160   period tested. However, the decrease of Y(NPQ) quantum yield and the significant increase in

161   Y(NO) quantum yield indicated that electrons underwent unregulated energy dissipation which

162   might induce free radicals and membrane damage at this low temperature (**Figure 2A**).

163   Measurements of CO_2 gas exchange showed that the reduced PSII activity, as determined by PAM

164   fluorometry was accompanied by a drastic decline of the CO_2 assimilation rate (*A*) at 4°C but not

165   at 12°C (**Figure 2B**). Transpiration rates (*E*) increased transiently in all three genotypes already at

166   12°C but more severely at 4°C. The elevated transpiration coincided with a chilling-dependent

167   increase in the leaf CO_2 concentration, indicating that despite increased stomata opening, activities

168   of Calvin cycle enzymes were greatly reduced (**Figure 2B**).

169   To gain insight into global cold-dependent gene expression of sugar beet source and sink tissues,

170   we performed RNA-seq analyses on leaf and taproot tissue of sugar beet plants from the above

171   genotypes exposed to cold (4°C) or control (20°C) conditions. Samples were collected 14 days

172   after transfer from 12°C to 4°C, i.e. when metabolic accumulation of sugars (**Figure 1**) and

173   photosynthetic rate were maximally contrasting. The obtained RNA-seq reads were mapped to the

174   sugar beet reference genome (Dohm et al., 2013). Transcriptome sequencing data has been

175   deposited in the GenBank Sequence Read Archive (BioProject PRJNA602804).

176   Exposure to cold induced global rearrangement of gene expression in both shoot and taproot tissues

177   (Supplemental Figure 1). We extracted transcript information on genes involved in photosynthesis.

178   In a PC analysis based on expression values in leaf tissue of genes annotated as 'photosynthesis',

179   'photosynthesis.lightreaction', 'photosynthesis.calvin cycle', or 'photosynthesis.photorespiration'

180   by Mapman Ontology for sugar beet, the PC1 separated the temperature treatments in the three

181   genotypes. PC1 explained 84.5%, PC2 7.1% of the variance in expression between 4°C and 20°C

182   within the genotypes (**Figure 2C**). Independent genotypes were not clearly separated and

183   accordingly, expression levels of photosynthesis-related genes behaved similarly in all three

184   genotypes (**Figure 2C**, Supplemental Figure 1). At 20°C, about 9% of all transcript reads of each

185   genotype could be assigned to 'photosynthesis' subgroups. After exposure to 4°C, this group was

186   represented by only 3% of all reads, indicating a drastic downregulation of photosynthesis-related

187   genes in the cold (**Figure 2D**). Downregulation of expression was for example observed for

188   transcripts with homology to genes encoding RubisCO activase (BvRCA), RubisCo small subunit

189   (BvRBCS), a Chlorophyll A/B binding protein (BvCABA), and Plastocyanin (BvPC) (**Figure 2E,**

6

190 **upper row**). Genes related to ROS processing on the other hand displayed differential regulation.

191 Whereas genes encoding Glutathione reductases were upregulated in the cold, genes encoding

192 Superoxide-dismutase or Ascorbate reductase were down- or not significantly regulated,

193 respectively (**Figure 2E, bottom row**). In summary, the data demonstrated that sugar beet

194 photosynthesis was extremely sensitive to chilling temperatures below 12°C and suggested that the

195 (hardly occurring) assimilation of CO_2 does not completely account for the increase in biomass and

196 sugar determined for leaves of cold-treated sugar beet (**Figure 1**).

Cold temperatures alter major carbohydrate metabolism in shoots and taproots

198 We investigated whether the reduction of taproot sucrose concentration in the cold could be

199 explained with increased respiration and whether cold conditions would result in differential

200 expression of genes involved in major carbohydrate metabolism **(Figure 3)**. Respiration in taproot

201 tissue was dependent on the examined part of the taproot, in that it decreased with increasing depths

202 of the surrounding soil **(Figure 3A)**. This position-dependent decrease in respiration (proportionate

203 to the depth of soil surrounding the respective part of the taproot) was also observed at 4°C,

204 however, in each part of the taproot, respiration was – in comparison to the corresponding control

205 – generally lower when sugar beets had been exposed to 4°C **(Figure 3A)**. This data suggested

206 that, in the cold, carbohydrates in the taproot were used for glycolytic and oxidative catabolism to

207 a lesser extent than under the 20°C control condition. In shoots, i.e. in source leaves of all

208 genotypes, on the contrary, respiration increased in the cold **(Figure 3B)**, indicating that the mature

209 leaves, which hardly assimilate CO_2 at this temperature **(Figure 2)**, had a high requirement for

210 carbohydrate supply from other sources. One of these sources was probably starch, which

211 decreased in leaves in the cold (**Figure 1**). PC and heat map analysis, loaded with expression values

212 of genes assigned as "major CHO metabolism", revealed organ- and temperature-dependent

213 differences **(Figure 3C**, **Figure 3D)**. The first principal component PC1 explained 66.9% of the

214 expression differences between roots and shoots and the PC2 accounted for 17.9% of the

215 differences in expression between 20°C and 4°C. Both organs showed clearer separation at 20°C

216 in comparison to 4°C **(Figure 3C)**. The heat map representation visualizes that expression levels

217 of genes contributing to starch degradation and synthesis in leaves were up- (starch degradation)

218 or downregulated (starch synthesis) by cold exposure, respectively. Despite extremely low starch

219 levels in taproots **(Figure 1)**, starch-related genes were also expressed and regulated in taproots

220 **(Figure 3D)**. This observation is in line with a report from Turesson et al (2014) who showed that

7

221 starch metabolic enzymes were active despite the lacking occurrence of starch in taproots
222 (Turesson et al., 2014).

223 Expression levels of sucrose synthesis genes were upregulated in roots in the cold but unchanged
224 in shoots. Sucrose degradation genes, however, were clearly downregulated in roots but slightly
225 upregulated in shoots (**Figure 3D**). Sucrose Phosphate Synthase (SPS) and Sucrose Synthase
226 (SUS) are key factors of sucrose biosynthesis and degradation and regulate carbohydrate
227 partitioning between source and sink tissues (Voll et al., 2014; Sturm, 1996; Martin et al., 1993;
228 Kovtun and Daie, 1995). A genome-wide search in the sugar beet genome (RefBeet 1.2, (Dohm et
229 al., 2013)) identified two SPS and four SUS isoforms. Bayesian analysis identified both SPS
230 isoforms as homologs of the Arabidopsis SPS 'A' subgroup (Voll et al., 2014) (Supplemental
231 Figure 3). The two SPS isoforms showed differential organ-specific and cold-dependent
232 expression. In shoots of all genotypes, expression of *SPSA1* was about 10-fold higher than in roots,
233 when plants had been exposed to 20°C. Cold treatment upregulated its expression in roots up to
234 sevenfold, but did not affect expression levels in the shoot. *SPSA2* expression at 20°C was low in
235 shoots but high in roots of all three tested genotypes. The expression of this isoform was previously
236 identified as taproot-specific, glucose-induced, and sucrose-repressed (Hesse et al., 1995). *SPSA2*
237 expression was also unaltered or even downregulated (in case of GT2) in shoots upon cold
238 treatment, but, as opposed to *SPSA1, SPSA2* expression was induced in taproots of all genotypes.
239 On the protein level, revealed by MS-based analysis of the soluble proteome from the very same
240 taproot tissues as was used for the transcriptome analysis, BvSPSA1 but not BvSPSA2 was slightly
241 upregulated. SPS activity, however, was higher under 4°C in comparison to 20°C in both protein
242 extracts from leaves and taproots (Supplemental Figure 3). Higher levels of UDP in taproots and
243 Sucrose-6-Phosphate in shoots in the cold in comparison to control temperatures along with the
244 elevated levels of the allosteric SPS activator G-6-P (Huber and Huber, 1992) supported a scenario
245 in which SPS activity was elevated in both roots and shoots (Supplemental Figure 3).

246 The expression of the four sucrose synthase isoforms showed tissue and temperature-dependent
247 differences. While *BvSUS1* and *BvSUS2* isoforms were strongly expressed in roots and their
248 corresponding proteins highly abundant, BvSUS3 and BvSUS4 were hardly expressed and their
249 corresponding proteins were not detected by MS in a soluble proteome fraction (**Figure 3E**,
250 Supplemental Figure 4). Both *BvSUS1* and *BvSUS2* were ten (*BvSUS1*) to hundredfold (*BvSUS2*)
251 higher expressed in roots in comparison to shoots. After the cold exposure period, mRNA levels

8

252 of both isoforms decreased about half in the roots. *BvSUS2* transcript levels in shoots increased ten

253 to twentyfold, however, without reaching the high levels in taproots (**Figure 3E**). BvSUS2, but not

254 BvSUS1 was also reduced at the protein level indicating differential protein turnover dynamics of

255 the two isoforms in the cold (Supplemental Figure 4).

256 To determine the cellular energy state of shoot and taproots, adenylate levels were measured

257 (**Figure 3F**). ATP, ATP/ADP ratio, and energy charge (EC = [ATP] + 0.5 [ADP]/[ATP] + [ADP]

258 + [AMP]) increased in shoots of all genotypes. This elevated energization of shoot tissue in the

259 cold can be explained by the drastic decrease in ATP-consuming CO_2 assimilation (**Figure 2B**)

260 and the increase of respiration in shoots (**Figure 3B**). On the other hand, energization of taproot

261 tissue did not change in the cold. Although ATP levels also increased, ATP/ADP ratios of GT1 and

262 GT2 taproots were unaltered or even decreased in GT3. Also EC of taproots did not increase in the

263 cold but rather decreased in tendency in GT2 and GT3 taproots (**Figure 3F**). Taken together, these

264 data indicate that developing taproots shifted in the cold from a sucrose consuming/storing towards

265 a sucrose synthesizing tissue and that leaves adopted – at least in part – characteristics of sink

266 tissues.

Cold temperatures reverse phloem translocation of sucrose and esculin

268 The above data indicated that cold-induced shoot sugar accumulation was not or only insufficiently

269 fueled by carbon dioxide assimilation, or starch degradation, and suggested that carbon used as

270 building block for shoot metabolites might be remobilized from taproot storage cells. To track the

271 fate of taproot-based carbon after exposure to cold temperatures, we directly fed taproot tissue with

272 radiolabeled ^{14}C-sucrose by injecting the substance from the exterior into the fleshy parenchymatic

273 taproot tissue of plants grown under 20°C control conditions or cold-exposed plants (5 days at 12°C

274 and then 7 days 4°C). The treated plants were then kept for one more week at control or cold

275 temperatures and then dissected into individual leaves and taproots. The leaves or longitudinal thin

276 sections of taproots were pressed and dried, and incorporated radioactivity was visualized using

277 phosphor imaging plates and software (**Figure 4**, Supplemental Figure 6, Supplemental Figure 7).

278 This analysis surprisingly revealed that plants grown under the 4°C condition showed distribution

279 of radioactivity in source leaves. Radioactivity in leaves of cold-treated plants was detected in leaf

280 veins and intensity gradually decreased towards the leaf tip indicating transport via the phloem

281 vessels (**Figure 4B**). In plants grown under control conditions, however, radioactivity could hardly

9

282 be detected in source leaves (**Figure 4C**). However, radioactivity was to some extent detectable in

283 young sink leaves of control plants and extractable from combined shoot petioles **(Figure 4D)**.

284 This radioactivity may represent xylem transported sucrose or derivatives due to injury of

285 punctuated vessels as a result of the invasive inoculation procedure. The drastic water loss in shoots

286 upon cold (**Figure 1**) however indicated that at 4°C radiolabeled sucrose was not efficiently

287 transported to prior source leaves via the xylem but rather via the phloem.

288 To test this hypothesis, we used a strategy less invasive to the organs/tissues examined later, and

289 more realistically mirroring the actual transport of assimilates (including the prior "downward"

290 transport. We loaded esculin, a phloem mobile coumarin glycoside (Knoblauch et al., 2015)

291 recognized by several sucrose transporters, including the *Beta vulgaris* phloem loader BvSUT1

292 (Nieberl et al., 2017) onto source leaves and assessed esculin transport routes directly via detection

293 of esculin-derived fluorescence in thin sections of leaf petioles of source leaves from the very same

294 plants, which had not been loaded with esculin, after transfer to cold or under control conditions.

295 Here we observed that blue esculin fluorescence was solely detected in phloem of vascular bundles

296 of source leaves from plants transferred to cold. However, the fluorescence was not only confined

297 to the phloem region but also detected to some small extent in a bundle region interspersed with

298 the yellow fluorescence of the lignified xylem vessels **(Figure 4)**. At 20°C, esculin fluorescence

299 was never detected in the phloem (**Figure 4**).

300 To follow sucrose flow directly from the site of inoculation in the taproots, we performed

301 longitudinal thin sections of taproots inoculated with the radiolabeled sucrose and exposed the

302 tissue to phosphor imaging plates (**Figure 4**, Supplemental Figure 6, Supplemental Figure 7).

303 Radioactivity in taproots from plants exposed to 4°C was detectable and concentrated in veiny or

304 spotty structures that resided between the site of inoculation and the taproot top (crown) tissue. At

305 higher magnification, these structures could be identified as vascular bundles (Supplemental

306 Figure 6). In taproots from plants grown under control conditions, no such distinct darkening of

307 vascular structures could be observed, although some observed blackening of crown tissue

308 indicated that radioactivity was also transported upwards into the direction of the

309 shoot (Supplemental Figure 7). However, in most cases, radioactivity in 20°C taproots was either

310 merely confined to parenchymatic regions near the site of inoculation or concentrated in thick

311 strands that reached from the site of inoculation towards the emergence of lateral roots. These

312 results indicated that radiolabeled sucrose and esculin – the latter first being translocated to the

10

313   base of the petiole of the loaded leaf and though (at least parts of) the taproot - were preferentially

314   transported from taproots into shoots in the cold but not under control conditions and suggested

315   that sucrose released from parenchymatic storage tissue was also transported in the same manner.

316   Vacuolar sucrose importer and exporter genes and proteins show opposite cold-dependent

317   expression

318   Next, we analyzed whether transport of sucrose from taproots to shoots in the cold could be

319   mediated by differential activity of vacuolar sucrose importers and exporters. In Arabidopsis,

320   vacuolar sucrose import and export are mediated by activity of TST1 and SUC4 transporters,

321   respectively (Schulz et al., 2011; Schneider et al., 2012). In sugar beet, the TST1 homolog

322   BvTST2;1 is responsible for vacuolar sucrose accumulation (Jung et al., 2015). TST2;1 expression

323   in the taproots of all tested genotypes greatly exceeds that in leaf tissue substantiating its role as

324   the sucrose loader of taproot parenchyma vacuoles (**Figure 5**). Interestingly, both mRNA and

325   protein abundance decreased significantly in all genotypes in taproots after cold

326   treatment (**Figure 5B**, Supplemental Figure 8).

327   Export of sucrose from the vacuole is presumably mediated by a SUC4/SUT4 family homolog. We

328   identified Bv5_124860_zpft.t1 as the unambiguous homolog to the Arabidopsis SUC4 isoform and

329   accordingly termed the corresponding transporter BvSUT4 (Supplemental Figure 10). N-terminal

330   fusions of the BvSUT4 coding sequence with GFP transiently transformed into *Beta vulgaris* or

331   Arabidopsis mesophyll protoplasts clearly indicated that BvSUT4 was a tonoplast located protein

332   (**Figure 5D**). BvSUT4 mRNA showed lower abundance in older plants in comparison to younger

333   ones (Supplemental Figure 9). In contrast, TST2;1 mRNA increased with progression of leaf

334   development confirming the suggested oppositional activities of the TST2;1 and SUT4 transport

335   proteins (Supplemental Figure 9). In the RNA-seq data from the cold-treated genotypes examined

336   in this study, SUT4 mRNA levels increased significantly in taproots in the cold (**Figure 5C**). These

337   data indicated that vacuolar taproot sucrose import was decreased and vacuolar taproot sucrose

338   release increased under cold conditions and suggested that the opposite regulation of BvTST2;1

339   and BvSUT4 in taproots was the underlying driving force for the accumulation and delivery of

340   sugars in shoots.

341

342

11

Expression of floral regulator genes is adjusted in the cold

343   The observed re-translocation of sucrose from taproots to shoots might represent a preparative

345   metabolic and genetic rearrangement for initiation of flowering. We therefore extracted

346   information on expression of flowering regulator genes and observed significant downregulation

347   of the floral repressor *BvFT1* and upregulation of the floral activator *BvFT2* in the cold in leaves

348   (**Figure 6**). These results agree with reports from Pin et al (2010), where cold treatment also

349   induced *FT2* and repressed *FT1* expression (Pin et al., 2012). The genotypes analyzed here have

350   biennial growth behavior thus BTC1 and BBX19 may not influence *FT1* expression. However,

351   these two genes were reciprocally cold regulated. While *BTC1* was downregulated in the cold,

352   *BBX19* was upregulated. In contrast to results from Pin et al. (2012), where vernalized biennials

353   had increased *BTC1* mRNA levels in comparison to non-vernalized plants (Pin et al., 2012), BTC1

354   was downregulated in the cold. However, in the mentioned study, expression was analyzed after

355   and not during early stages of vernalization. We found that *BTC1* and *BBX19* were expressed in

356   both, shoots and taproots, and expression of *BBX19* in taproots exceeded that in the shoot at 20°C

357   almost threefold. However, potential targets of these encoded loss-of-function proteins, *FT1* and

358   *FT2* were specifically and exclusively expressed in leaf tissue (**Figure 6**). In summary, these data

359   showed that the vernalization process was already transmitted to the expression level of floral

360   regulator genes and that transcriptional changes of related genes did occur in both, shoots and

361   taproots.

12

Discussion

In this work we discovered a so far unknown switch of sink and source identities of taproots and shoots upon cold exposure of sugar beet plants. In contrast to sinks like seeds, culms or tubers, which adopt source identities after complete differentiation and subsequent separation from their nourishing source, the sink-source switch in sugar beet occurred in response to an environmental stimulus when both shoot and taproot tissues were still physiologically connected.

At 4°C, shoot CO_2 assimilation was drastically reduced but PSII activity stayed relatively high **(Figure 2).** This correlation indicates that enzymes of the Calvin-Benson cycle slowed down in the cold and could not utilize electrons liberated from the photosynthetic electron transport (PET) chain. During the decreased CO_2 fixation rates at cold conditions, high PET rates may have detrimental effects because they produce harmful reactive oxygen species (ROS) like super-oxide, hydrogen peroxide or hydroxyl anions (Suzuki and Mittler, 2006; Choudhury et al., 2017; Pommerrenig et al., 2018). During the cold exposure kinetic (**Figure 1 and Figure 2**), we recorded decreased CO_2 assimilation already at 12°C. As indicated by the increased Y(NPQ) percentage (**Figure 2A**), the Mehler-Ascorbate Pathway (Asada, 1999) might act as an additional quencher for PET-released electrons at this temperature. At 4°C, this scavenging pathway apparently also slowed down, as indicated by the further decrease in Y(II) but also Y(NPQ), and the concomitant increase in Y(NO). The significant increase in Y(NO) at 4°C is indicative for non-regulated energy dissipation, which can severely damage chloroplast membranes and plant cells in a cold- and high light dependent manner. Under those sustained challenging conditions, the cold response was apparently transduced to the level of gene expression where it led to an effective downregulation of transcripts of photosynthesis-related genes **(Figure 2D and 2E)**. Induction of glutathione reductase genes supported a scenario in which leaves induced cellular counter measures against light-induced electron overflow at the photosystems and damages of chloroplasts **(Figure 2E)**.

These data are in agreement with results from Arabidopsis, where photosynthesis as well as expression of *RBCS* and *CAB* genes were significantly reduced after shifting of 23°C-grown plants to 5°C, although photosynthesis recovered after prolonged exposure to cold (Strand et al., 1997). In summary, these metabolic and transcriptomic changes would eventually result in drastic decrease of CO_2 incorporation into sugars, which are required for growth and protection of cell vitality in the cold.

13

392   Despite inactivation of photosynthesis, however, sugars continued to accumulate in leaves and
393   decreased in taproots in the cold **(Figure 1)**. Decreasing sucrose levels in taproots and impaired
394   respiration in root tissue indicated that sucrose was not used for energy metabolism during cold at
395   the same rate as under control conditions in the taproot **(Figure 3)**. Cold tolerant plants like
396   Arabidopsis accumulate sugars in leaves in the cold by maintaining photosynthetic activity,
397   reducing sucrose phloem loading, and increasing sugar import into leaf vacuoles (Wingenter et al.,
398   2010; Nägele and Heyer, 2013). While Arabidopsis has the ability to overcome sugar repression of
399   photosynthesis after prolonged exposure to cold (Huner et al., 1993; Strand et al., 1997), such
400   mechanism apparently does not occur in sugar beet in the same manner. In contrast, the drastic
401   decrease of photosynthetic activity in the shoot rather turned leaves into sink organs, which were
402   supplied with sugar from taproots **(Figure 4)**.

403   Under non-chilling temperatures, reversibility of taproot sink and remobilization of sugars from
404   storage vacuoles might become essential when leaves have to re-grow after wounding of the shoot
405   caused by e.g. feeding damage or when a new strong sink like the inflorescence is formed after
406   winter. However, as indicated by the movement of radiolabeled sucrose and fluorescent esculin
407   towards the shoot, and therefore to previous source leaves also early cold response triggered a
408   remobilization of carbohydrates from taproot storage **(Figure 4)**. While sucrose biosynthesis and
409   hydrolysis were reciprocally regulated under warm and cold conditions **(Figure 3)**, levels of taproot
410   sucrose decreased upon cold treatment (**Figure 1**). In agreement with this process, we identified
411   opposing regulation of the major vacuolar sucrose importer (BvTST2;1) and putative major
412   exporter (BvSUT4) in the same tissue (**Figure 5**). BvTST2;1 expression and protein abundance
413   was significantly downregulated, while, in contrast, BvSUT4 was upregulated in the cold. The role
414   of BvSUT4 as an exporter of sucrose is supported by its general homology to sucrose transporters
415   of the SUC/SUT family and by its homology to AtSUC4 (**Figure 5**), for which both sucrose export
416   activity and vacuolar localization have been shown (Schulz et al., 2011; Schneider et al., 2012). It
417   seems unlikely that sugars are released from vacuoles in the cold as monosaccharides via other
418   transporters, e.g. by the already described BvIMP protein (Klemens et al., 2014). This is because
419   vacuolar invertases - a prerequisite for vacuolar monosaccharide generation and thus export – are
420   hardly active at the analyzed developmental stage (Giaquinta, 1979; Godt and Roitsch, 2006).

421   The previously explained findings are schematically explained in the following model **(Figure 7)**.

422 It is surprising that flux transition occurred already pre-bolting i.e. before the formation of an
423 inflorescence that would then act as new sink organ utilizing remobilized taproot sugars as building
424 blocks. During the early phases of vernalization warmer temperatures or longer daylight, additional
425 prerequisites for bolting (Mutasa-Göttgens et al., 2010; Ritz et al., 2010), do not yet signal onset
426 of spring. However, simultaneously to the switching of identities, the cold exposure also led to
427 adjustment of expression levels of floral regulator genes. *FT1* and *FT2*, the floral repressor and
428 activator genes (Pin et al., 2010), respectively, showed reciprocal regulation in the cold in shoots
429 **(Figure 6)**. The expression of the flowering-related genes *BTC1* and *BBX19* in taproot tissue
430 suggested that taproots might also be involved in the perception of vernalization. It is tempting to
431 think into a direction where newly identified (Pfeiffer et al., 2014; Broccanello et al., 2015;
432 Tränkner et al., 2017) or yet undiscovered bolting loci might harbor yet uncharacterized factors
433 which might integrate both, bolting and required sink-source transition, similar to the recently
434 described FT homolog StSPS6A ('tuberigen') in potato (Navarro et al., 2011; Abelenda et al.,
435 2019).

436 Our study represents a comprehensive analysis of sugar beet taproot tissue during cold treatment
437 and shows that cold temperatures induce a sink to source transition, which establishes accumulation
438 of taproot-based carbohydrates in the shoot. For this, sugars have to be loaded into taproot phloem,
439 transported from taproots to shoots, and unloaded in leaf tissue. Currently it is unknown whether
440 taproot phloem loading in the cold involves an apoplastic step, whether the same phloem vessels
441 are being used for root- and shoot-bound sugar trafficking, and how sugar unloading is established
442 in former source leaves. Latter issue possibly involves a reprogramming of transporter activity that
443 could mediate sugar efflux from the vasculature to the mesophyll involving both passive and active
444 transport processes. Our transcriptomic and proteomic approach might reveal candidate factors and
445 transporters involved in this unloading in the cold in the future.

446 The findings also have implications for agriculture and breeding, where attempts have been made
447 to grow sugar beet over all seasons (Hoffmann and Kluge-Severin, 2011; Hoffmann and Kenter,
448 2018), a scenario which will become more and more realistic by the generation and employment
449 of bolting-resistant hybrid genotypes (Pin et al., 2010; Pfeiffer et al., 2014; Tränkner et al., 2016).
450 In addition, biennial growth of sugar beet might become facilitated by the increasing occurrence of
451 climate change-induced "warm" winters in e.g. middle and Northern Europe (Lavalle et al., 2009)
452 that would allow cultivation of sugar beet under non-freezing, non-lethal low temperatures.

15

453 However, even under non-freezing, but prolonged above zero chilling conditions, the advantages

454 of a longer vegetation period would be negated, at least to some extent, by the herein described

455 trade-off of cold-induced taproot sugar loss. This phenomenon might also partially account for the

456 observed reduced yield and higher marc to sugar ratio of autumn- or early spring-sown sugar beet

457 plants (Hoffmann and Kluge-Severin, 2011).

458 In future, it will be highly valuable to analyze this observed sink-source transition of taproots in

459 bolting resistant mutants without the activating function of FT2 (Pin et al., 2010) to reveal whether

460 FT activity is required for triggering this transition. Equally relevant will be the generation of

461 BvSUT4 mutant plants to study effects of lacking vacuolar sucrose efflux for floral induction and

462 cold tolerance. Such modified plants would possibly exhibit a diminished taproot sucrose release

463 and therefore a reduced building block supply for inflorescence formation. This potential impact

464 on bolting makes BvSUT4 a highly relevant target for breeding approaches (Pfeiffer et al., 2014;

465 Chiurugwi et al., 2013) aiming at bolting resistance and at withholding cold-induced sucrose loss

466 from taproots.

Materials and Methods

Plant Material and Growth conditions

469 Three hybrid sugar beet genotypes (GT1, GT2, GT3; KWS SAAT SE, Germany) were used for

470 this study. Plants were germinated and grown on standard soil substrate ED73 (Einheitserdwerke

471 Patzer, Germany)/ 10% (v/v) sand mixture under a 10 h light/14 h dark regimen, 60% relative

472 humidity, and 110 µmol m^{-2} s^{-1} light intensity. For growth- and sugar accumulation kinetics, plants

473 were grown for 6 weeks at 20°C, transferred for 1 week at 12°C and then 3 weeks at 4°C. For

474 RNA-seq and proteome analysis, plants were grown for 10 weeks at 20°C, transferred for 1 week

475 at 12°C and then 2 weeks at 4°C. Control plants were kept at 20°C. For harvest, plants were

476 dissected into shoot and taproot tissues. 4 pools out of three different plants were made for each

477 tissue. Tissues were chopped with a kitchen knife, transferred to liquid nitrogen, and kept at -80°C

478 until further processing.

Chlorophyll Fluorescence Measurements

480 Photosynthetic activity was measured using an Imaging-PAM *M-Series*-System (Heinz Walz,

481 Effeltrich, Germany). Plants were placed in the dark for 12 min to deplete the energy of PSII.

16

482 Capacity of PSII was measured by saturation with 14 cycles of PAR 76 (µmol photons m^{-2} s^{-1})

483 light-pulses at 0s, 50s, and 70s. Recorded fluorescence was used for calculation of effective

484 quantum yield of PSII [$Y(II) = (Fm'-F)/Fm'$], quantum yield of non-photochemical quenching

485 [$Y(NPQ) = 1 - Y(II) - 1/(NPQ+1+qL(Fm/Fo-1))$] and of non-regulated energy dissipation [$Y(NO)$

486 $= 1/(NPQ+1+qL(Fm/Fo-1))$]. Required factors were calculated by the formulas [$NPQ = (Fm-$

487 $Fm')/Fm'$], [$qN = (Fm-Fm')/(Fm-Fo')$], [$Fo' = Fo/ (Fv/Fm + Fo/Fm')$], [$qP = (Fm'-F)/(Fm'-Fo')$]

488 and [$qL = (Fm'-F)/(Fm'-Fo') \times Fo'/F = qP \times Fo'/F$].

Gas Exchange Measurements

490 A GFS-3000 system (Heinz Walz, Effeltrich, Germany) was employed to analyze gas exchange-

491 related parameters. A 2.5 cm^2 gas exchange cuvette was used to measure CO_2-assimilation rate,

492 respiration, leaf CO_2 concentration, and transpiration of sugar beet source leaf. Leaf regions

493 including large central mid ribs were omitted. The conditions inside of the cuvette were set to the

494 same temperature, humidity and CO_2-concentration the plants had been grown at. Measurement

495 sequence is listed in **Table 1**. The listed intervals were determined by a trial-experiment, in which

496 the time necessary for stabilization of the flow of CO_2 after transfer of the leaf section into the

497 cuvette and adoption to the changed light-intensities was measured. The measurement was started

498 after stabilization of the CO_2-flow, which required about 5 minutes. Measurements were performed

499 with 4 plants in 3 technical (repeated measurements of the same plant) replicates over a time of

500 1 min for each condition to account for variation caused by observed natural leaf-fluctuation and

501 leaf area outside of the cuvette. The 30 second interval between the measurements was necessary

502 for the leaf to return to the stabilized value.

503 **Table 1:** Sequence for gas-exchange measurements

time [s]	Light-intensity	measurement
+0	PAR 0	
+220	PAR 0	photosynthetic activity
+30	PAR 0	photosynthetic activity
+30	PAR 0	photosynthetic activity
+460	PAR 125	respiration/transpiration (light)
+30	PAR 125	respiration/transpiration (light)

17

+30	PAR 125	respiration/transpiration (light)
+320	PAR 0	respiration/transpiration (dark)
+30	PAR 0	respiration/transpiration (dark)
+30	PAR 0	respiration/transpiration (dark)

Respiration of sugar beet taproot tissue

Respiration of taproots was measured by cutting out 0.5 cm^2 tissue cubes from central taproot regions and measuring CO_2 production in a whole-plant cuvette with a volume of 60 cm^3. Values were normalized to tissue weight.

RNA extraction and sequencing

RNA was isolated from three biological replicates per genotype, tissue (leaf and root, respectively) and treatment, respectively. About 100 mg frozen plant material were pulverized in a tissue lyser (Qiagen, Hilden, Germany) at 30 Hz for 90 sec. After grinding, samples were again transferred to liquid N_2, supplemented with 1.5 ml QIAzol Lysis reagent (Qiagen, Hilden, Germany), vortexed three times for 30 sec, and centrifuged at 4 °C for 10 min at 12,000 g. Supernatants were transferred to fresh tubes, incubated at room temperature (RT) for 5 min, extracted with 300 µl chloroform, vortexed for 15 sec, and centrifuged at 4 °C for 15 min at 12,000 g. Aqueous supernatants were transferred to fresh tubes and RNA precipitated with 750 µl isopropanol for 10 min at RT and spun down at 4 °C for 10 min at 12,000 g. Precipitates were washed with 75% EtOH and the RNA pellets dried at 37 °C for 5-10 min prior to resuspension in 100 µl DEPC-H_2O by gentle shaking at 37 °C for 5-10 min. To remove residual contaminants, RNA was further purified using the RNeasy KIT (Qiagen, Hilden, Germany). Per 100 µL RNA suspension, 350 µl RLT buffer (provided with the kit) were added and vortexed briefly. Then, 250 µl ethanol were added and the mixture was vortexed again. The RNA was spin-column purified and finally eluted from the column for a final volume of 50 µl (in DEPC-H_2O) per sample. The RNA was quantified (NanoDrop 2000/2000c, Thermo Fisher) for each sample prior to further processing or storage at -80 °C. RNA quality was confirmed using an Agilent Technologies 2100 Bioanalyzer (Palo Alto, CA, USA). RNAs (2 µg per sample) were transcribed to cDNAs and sequenced using an Illumina, Inc. HiSeq 2000 system. Sequencing and assembly were provided as a custom service (GATC GmbH, Konstanz, Germany). The statistical analysis process included data normalization, graphical exploration of raw and normalized data, test for differential expression for each feature between the conditions and raw p-

18

530   value adjustment. The analysis was performed using the R software (Team, 2017), Bioconductor

531   (Gentleman et al., 2004) packages including DESeq2 (Anders and Huber, 2010; Love et al., 2014)

532   and the SARTools package developed at PF2 – Institute Pasteur.

533   **Phylogenetic analysis**

534   Multiple sequence alignments of amino acid sequences were performed using Clustal Omega

535   (Sievers et al., 2011). Bayesian phylogenetic analysis was performed with MrBayes version 3.2

536   (Ronquist et al., 2012). MrBayes always selected the best-fit models 'Jones' (Jones et al., 1992)

537   and 'WAG' (Whelan and Goldman, 2001) for amino acid substitution analysis of SPS proteins and

538   SUS proteins, respectively. MrBayes conducted two parallel Metropolis coupled Monte Carlo

539   Markov chain analysis with four chains for 300,000 generations. Trees were sampled every 1,000

540   generations. The analyses were run until the standard deviation of split frequencies were below

541   0.005. Consensus trees were computed after burn-in of the first 25% of trees and visualized using

542   FigTree version 1.4.3.

543   **PCA and heatmap analysis**

544   For RNAseq data the mean cpm values were used for the analysis. Data were visualized using

545   ClustVis (Metsalu and Vilo, 2015).

546   **Analysis of soluble sugars and starch**

547   Leaves and taproots were harvested separately, frozen in liquid nitrogen, freeze-dried and stored at

548   -80°C until use. Pulverized material was extracted twice with 1 ml 80% EtOH at 80°C for 1 h.

549   Combined extracts were evaporated in a vacufuge concentrator (Eppendorf, Hamburg, Germany)

550   and pellets were resolved in ddH$_2$O. For starch isolation pellets were washed with 80% EtOH and

551   1 ml ddH$_2$0. 200 µl water were added to the pellet and the sample was autoclaved for 40 min at

552   121°C. 200 µl enzyme-mix (5 U α-Amylase; 5 U Amyloglucosidase in 200 mM Sodium-Acetate

553   pH 4.8) were added to the pellet and starch was hydrolytically cleaved into glucose-units at 37°C

554   for 4 h. The enzymatic digestion was stopped by heating the samples to 95°C for 10 min. After

555   centrifugation (20,000 *g*; 10 min; 21°C) the supernatant could be used for starch quantification.

556   Extracted sugars and hydrolytically cleaved starch were quantified using a NAD+-coupled

557   enzymatic assay (Stitt et al., 1989).

558   **Analysis of phosphorylated metabolites**

19

559   The contents of phosphorylated intermediates (Glucose-6-Phosphate, Fructose-6-Phosphate,

560   Sucrose-6-Phosphate, UDP-Glucose, UDP) were determined according to (Horst et al., 2010).

561   **Radiolabeled sucrose translocation assay**

562   Ten- to 12-week old sugar beet plants grown at 20°C under short day conditions (10 h light, 14 h

563   darkness) were used for the analysis. Plants for cold-treatment were grown for 1 more week at

564   12°C and then kept for 6 to 7 days at 4°C. Taproots from 4°C and 20°C plants were partially

565   uncovered from surrounding soil substrate and a 1 mm hole punched with a biopsy stance into the

566   upper half of the taproot (approximately 1 cm below the soil surface). The created pit was filled

567   with 10 µl of 1 to 2 diluted radiolabeled sucrose (536 mCi/mmol) (Hartmann Analytic,

568   Braunschweig, Germany) and coated with a drop of Vaseline. Plants were then kept for another 10

569   days at 4°C or 20°C (control). At the end of the treatment, all source leaves of injected plants were

570   detached and individually pressed between blotting paper. For detection of radioactivity in taproots,

571   taproots were dug out, washed and cut in thin slices (approximately 0.5 mm thick) with a truffle

572   slicer and pressed between blotting paper. Radioactivity was recorded with Phosphor-Image plates

573   (exposed for 4 to 5 h to adaxial surface of pressed and dried leaves or to dried taproot slices) and

574   plates were analyzed with a Cyclone Storage Phosphor Screen (Packard Bioscience, Meriden, CT,

575   USA). For quantification of radioactivity in petioles, source leaf petioles from the same leaves used

576   for phosphoimaging were cut off, ground, and pulverized. 5 to 10 mg powder were mixed with 2

577   ml scintillation cocktail and counts per minute (cpm) recorded with a TRI-Carb 2810TR liquid

578   scintillation analyzer (Perkin Elmer, Waltham, MA, USA).

579   *In planta* **esculin transport**

580   Ten-week old sugar beet plants grown at 20°C under short day conditions (10 h light, 14 h darkness)

581   were used for the analysis. One source leaf per plant (usually from leaf stage 10 to 12) was abraded

582   at the adaxial side with fine sandpaper (grade 800). About 500 µl of a 100 mM esculin

583   sesquihydrate (Carl Roth, Karlsruhe, Germany) solution was distributed over the injured leaf

584   surface with a plastic pipette. Treated leaves were coated with plastic foil, kept for 2 more days at

585   20°C and then transferred to 4°C or kept at 20°C (control). After 5 to 7 days in the cold, not esculin-

586   loaded source leaves were detached and sections of petioles were analyzed for esculin fluorescence

587   with a Leica TCS SP5II confocal microscope (Leica, Mannheim, Germany) using a HCX PL APO

588   lamda blue 20.0x0.70 IMM UV objective. Slices of taproots from the very same plants were

20

589 analyzed for esculin fluorescence to ensure that esculin was successfully translocated into taproots

590 in both cold-treated and control plants. The emission bandwidths were 440 – 465 nm for detection

591 of esculin fluorescence and 594 – 631 nm for lignin fluorescence.

Soluble protein extraction

593 Plants were harvested, washed, and separated in the cold into taproots and source leaves. Frozen

594 leaf-tissue was pulverized with N_2(l) using a Retsch mill (Retsch GmbH, Germany). 800 µl buffer

595 E1 (50 mM HEPES-KOH pH 7.5, 10 mM $MgCl_2$, 1 mM EDTA pH 7.5, 2 mM DTT, 1 mM PMSF,

596 1 mM Pefabloc, 5 mM aminohexanoic acid, 0,1% (v/v) Triton X-100, 10% (v/v) glycerol) were

597 transferred to 100 mg of pulverized tissue into 1.5 ml Eppendorf cups. Samples were vortexed and

598 centrifuged for 3 min at 12.000g at 4°C. 500 µL of the supernatant were loaded onto a Sephadex

599 NAP5 (G25) column (GE Health Care, United Kingdom), pre-equilibrated with buffer E1 w/o

600 Triton X-100. Eluents were collected in precooled Eppendorf cups and stored at -20°C. Taproot

601 tissues were treated as above with the following alterations: Taproots were blended with buffer E1

602 at 4°C until a homogenous pulp was obtained. The pulp was roughly filtered through a kitchen

603 sieve and centrifuged. 5 ml of the supernatant were dialyzed trough a membrane with 12 kDa pore

604 size for 48 h against 2 L ddH_2O. Water was exchanged seven to eight times. Samples were collected

605 in precooled Eppendorf cups and used for enzymatic tests or stored at -20°C. Liquid

606 chromatography and tandem mass spectrometry was performed as described in (Jung et al., 2015).

Isolation of taproot vacuoles and vacuolar proteins

608 Vacuoles were isolated as described by (Jung et al., 2015).

Sucrose Phosphate Synthase assay

610 80 µg of soluble protein were added to 200 µl freshly prepared E_{max} (50 mM HEPES-KOH pH 7.5,

611 20 mM KCl, 4 mM $MgCl_2$, 12 mM UDP-Glc, 10 mM Frc-6-P : Glc-6-P (1:4)) , E_{lim} (50 mM

612 HEPES-KOH pH 7.5, 20 mM KCl, 4 mM $MgCl_2$, 4mM UDP-Glc, 2mM Frc-6-P : Glc-6-P (1:4), 5

613 mM KH_2PO_4) and E_{blank} (= E_{max} w/o UDP-glucose and sugar-phosphates), respectively. Samples

614 were incubated for 20 min at 25°C, followed by 5 min at 95°C to stop the reaction and centrifuged

615 at 12.000 g at 4°C for 5min. 100 µL of the supernatant were pipetted to 100 µL 5 M KOH and

616 incubated 10 min at 95°C. The solution was mixed with 800 µL anthrone (14.6 M H_2SO_4, 0,14%

617 (w/v) anthrone) and absorbance immediately measured at 620 nm. A calibration-standard was

618 made with 0-5 mmol sucrose.

21

619 **Subcellular localization of BvSUT4 in Arabidopsis and sugar beet mesophyll protoplasts**

620 The BvSUT4 CDS (Bv5_124860_zpft.t1= BVRB_5g124860) was amplified from *B. vulgaris* leaf

621 RNA with the gene specific primers BvSUT4-CACC-f (5'-CAC CAT GAC AGG CCA GGA CCA

622 AAA TA-3') and BvSUT4-rev (5'-TAC ATG CAT CAC ATG AAC TCT GG-3'). The resulting

623 open reading frame was cloned into pENTR/D-TOPO (Life Technologies, Darmstadt, Germany),

624 sequenced and recombined into the Gateway-compatible destination vector pK7FWG,0 (Karimi et

625 al., 2002) to obtain a p*35S::BvSUT4-GFP* fusion. Transient transformation of A. thaliana

626 mesophyll protoplasts was performed as described (Abel and Theologis, 1994). Isolation and

627 transient transformation of *B. vulgaris* mesophyll protoplasts were performed as described (Nieberl

628 et al., 2017).

629 **Data availability**

630 Transcriptome sequencing data has been deposited in the GenBank Sequence Read Archive under

631 BioProject PRJNA602804.

632 # Acknowledgements

637 # Author contributions

638 H.E.N., F.L., W.K., K.H., U.S., B.P., designed the research;

639 C.M.R., C.M., I.K., W.Z., F.R., P.N., B.P performed research;

640 O.C., J.M.C.G, T.M. contributed new analytic/computational/etc. tools;

641 C.M.R., C.M., B.P., analyzed data;

642 B.P., C.M., and H.E.N. wrote the paper.

References

Abel, S. and Theologis, A. (1994). Transient transformation of Arabidopsis leaf protoplasts: a versatile experimental system to study gene expression. The Plant Journal **5**: 421–427.

Abelenda, J.A., Bergonzi, S., Oortwijn, M., Sonnewald, S., Du, M., Visser, R.G., Sonnewald, U., and Bachem, C.W. (2019). Source-Sink Regulation Is Mediated by Interaction of an FT Homolog with a SWEET Protein in Potato. Current Biology.

Anders, S. and Huber, W. (2010). Differential expression analysis for sequence count data. Genome biology **11**: R106.

Asada, K. (1999). The water-water cycle in chloroplasts: scavenging of active oxygens and dissipation of excess photons. Annual review of plant biology **50**: 601–639.

Asada, K., Endo, T., Mano, J., and Miyake, C. (1998). Molecular mechanisms for relaxation of and protection from light stress. In 'Stress responses of photosynthetic organisms'.(Eds K Saton, N Murata) pp. 37–52 (Elsevier: Amsterdam).

Boussiengui-Boussiengui, G., Groenewald, J.-H., and Botha, F.C. (2016). Metabolic changes associated with the sink-source transition during sprouting of the axillary buds on the sugarcane culm. Tropical Plant Biology **9**: 1–11.

Broccanello, C., Stevanato, P., Biscarini, F., Cantu, D., and Saccomani, M. (2015). A new polymorphism on chromosome 6 associated with bolting tendency in sugar beet. BMC Genetics **16**: 142.

Chen, L.-Q., Qu, X.-Q., Hou, B.-H., Sosso, D., Osorio, S., Fernie, A.R., and Frommer, W.B. (2012). Sucrose Efflux Mediated by SWEET Proteins as a Key Step for Phloem Transport. Science **335**: 207.

Chiurugwi, T., Holmes, H.F., Qi, A., Chia, T.Y., Hedden, P., and Mutasa-Göttgens, E.S. (2013). Development of new quantitative physiological and molecular breeding parameters based on the sugar-beet vernalization intensity model. The Journal of Agricultural Science **151**: 492–505.

Choudhury, F.K., Rivero, R.M., Blumwald, E., and Mittler, R. (2017). Reactive oxygen species, abiotic stress and stress combination. The Plant Journal **90**: 856–867.

Dally, N., Xiao, K., Holtgräwe, D., and Jung, C. (2014). The *B2* flowering time locus of beet encodes a zinc finger transcription factor. Proc Natl Acad Sci USA **111**: 10365.

Dohm, J.C. et al. (2013). The genome of the recently domesticated crop plant sugar beet (Beta vulgaris). Nature **505**: 546.

Gentleman, R.C., Carey, V.J., Bates, D.M., Bolstad, B., Dettling, M., Dudoit, S., Ellis, B., Gautier, L., Ge, Y., and Gentry, J. (2004). Bioconductor: open software development for computational biology and bioinformatics. Genome biology **5**: R80.

Giaquinta, R.T. (1979). Sucrose translocation and storage in the sugar beet. Plant Physiol **63**.

676   **Godt, D. and Roitsch, T.** (2006). The developmental and organ specific expression of sucrose cleaving
677   enzymes in sugar beet suggests a transition between apoplasmic and symplasmic phloem
678   unloading in the tap roots. Plant Physiology and Biochemistry **44**: 656–665.

679   **Gottwald, J.R., Krysan, P.J., Young, J.C., Evert, R.F., and Sussman, M.R.** (2000). Genetic evidence for the
680   *in planta* role of phloem-specific plasma membrane sucrose transporters. Proc Natl Acad Sci USA
681   **97**: 13979.

682   **Herbers, K. and Sonnewald, U.** (1998). Molecular determinants of sink strength. Current Opinion in Plant
683   Biology **1**: 207–216.

684   **Hesse, H., Sonnewald, U., and Willmitzer, L.** (1995). Cloning and expression analysis of sucrose-
685   phosphate synthase from sugar beet (Beta vulgaris L.). Molecular and General Genetics MGG
686   **247**: 515–520.

687   **Hoffmann, C.M. and Kenter, C.** (2018). Yield Potential of Sugar Beet – Have We Hit the Ceiling? Frontiers
688   in Plant Science **9**: 289.

689   **Hoffmann, C.M. and Kluge-Severin, S.** (2011). Growth analysis of autumn and spring sown sugar beet.
690   European Journal of Agronomy **34**: 1–9.

691   **Horst, R.J., Doehlemann, G., Wahl, R., Hofmann, J., Schmiedl, A., Kahmann, R., Kämper, J., Sonnewald,**
692   **U., and Voll, L.M.** (2010). *Ustilago maydis* Infection Strongly Alters Organic Nitrogen Allocation in
693   Maize and Stimulates Productivity of Systemic Source Leaves. Plant Physiol. **152**: 293.

694   **Huber, S.C. and Huber, J.L.** (1992). Role of Sucrose-Phosphate Synthase in Sucrose Metabolism in Leaves.
695   Plant Physiol. **99**: 1275.

696   **Huner, N.P.A., Öquist, G., Hurry, V.M., Krol, M., Falk, S., and Griffith, M.** (1993). Photosynthesis,
697   photoinhibition and low temperature acclimation in cold tolerant plants. Photosynthesis
698   Research **37**: 19–39.

699   **Imlau, A., Truernit, E., and Sauer, N.** (1999). Cell-to-cell and long-distance trafficking of the green
700   fluorescent protein in the phloem and symplastic unloading of the protein into sink tissues. The
701   Plant Cell **11**: 309–322.

702   **Jones, D.T., Taylor, W.R., and Thornton, J.M.** (1992). The rapid generation of mutation data matrices
703   from protein sequences. Bioinformatics **8**: 275–282.

704   **Jung, B. et al.** (2015). Identification of the transporter responsible for sucrose accumulation in sugar beet
705   taproots. Nature Plants **1**: 14001.

706   **Karimi, M., Inzé, D., and Depicker, A.** (2002). GATEWAY™ vectors for Agrobacterium-mediated plant
707   transformation. Trends in plant science **7**: 193–195.

708   **Klemens, P.A.W., Patzke, K., Trentmann, O., Poschet, G., Büttner, M., Schulz, A., Marten, I., Hedrich, R.,**
709   **and Neuhaus, H.E.** (2014). Overexpression of a proton-coupled vacuolar glucose exporter
710   impairs freezing tolerance and seed germination. New Phytologist **202**: 188–197.

24

711   **Knoblauch, M., Vendrell, M., de Leau, E., Paterlini, A., Knox, K., Ross-Elliot, T., Reinders, A., Brockman,**
712   **S.A., Ward, J., and Oparka, K.** (2015). Multispectral Phloem-Mobile Probes: Properties and
713   Applications. Plant Physiol. **167**: 1211.

714   **Kovtun, Y. and Daie, J.** (1995). End-Product Control of Carbon Metabolism in Culture-Grown Sugar Beet
715   Plants (Molecular and Physiological Evidence on Accelerated Leaf Development and Enhanced
716   Gene Expression). Plant Physiol. **108**: 1647.

717   **Lavalle, C., Micale, F., Houston, T.D., Camia, A., Hiederer, R., Lazar, C., Conte, C., Amatulli, G., and**
718   **Genovese, G.** (2009). Climate change in Europe. 3. Impact on agriculture and forestry. A review.
719   Agronomy for Sustainable Development **29**: 433–446.

720   **Liu, B., Zhang, N., Wen, Y., Jin, X., Yang, J., Si, H., and Wang, D.** (2015). Transcriptomic changes during
721   tuber dormancy release process revealed by RNA sequencing in potato. Journal of Biotechnology
722   **198**: 17–30.

723   **Love, M.I., Huber, W., and Anders, S.** (2014). Moderated estimation of fold change and dispersion for
724   RNA-seq data with DESeq2. Genome biology **15**: 550.

725   **Ludewig, F. and Sonnewald, U.** (2016). Demand for food as driver for plant sink development. Journal of
726   Plant Physiology **203**: 110–115.

727   **Martin, T., Frommer, W.B., Salanoubat, M., and Willmitzer, L.** (1993). Expression of an Arabidopsis
728   sucrose synthase gene indicates a role in metabolization of sucrose both during phloem loading
729   and in sink organs. The Plant Journal **4**: 367–377.

730   **Metsalu, T. and Vilo, J.** (2015). ClustVis: a web tool for visualizing clustering of multivariate data using
731   Principal Component Analysis and heatmap. Nucleic acids research **43**: W566–W570.

732   **Mutasa-Göttgens, E.S., Qi, A., Zhang, W., Schulze-Buxloh, G., Jennings, A., Hohmann, U., Müller, A.E.,**
733   **and Hedden, P.** (2010). Bolting and flowering control in sugar beet: relationships and effects of
734   gibberellin, the bolting gene B and vernalization. AoB Plants **2010**.

735   **Nägele, T. and Heyer, A.G.** (2013). Approximating subcellular organisation of carbohydrate metabolism
736   during cold acclimation in different natural accessions of Arabidopsis thaliana. New Phytologist
737   **198**: 777–787.

738   **Navarro, C., Abelenda, J.A., Cruz-Oró, E., Cuéllar, C.A., Tamaki, S., Silva, J., Shimamoto, K., and Prat, S.**
739   (2011). Control of flowering and storage organ formation in potato by FLOWERING LOCUS T.
740   Nature **478**: 119.

741   **Nieberl, P. et al.** (2017). Functional characterisation and cell specificity of BvSUT1, the transporter that
742   loads sucrose into the phloem of sugar beet (Beta vulgaris L.) source leaves. Plant Biology **19**:
743   315–326.

744   **O'neill, B.P., Purnell, M.P., Kurniawan, N.D., Cowin, G.J., Galloway, G.J., Nielsen, L.K., and Brumbley,**
745   **S.M.** (2013). Non-Invasive Monitoring of Sucrose Mobilization from Culm Storage Parenchyma by
746   Magnetic Resonance Spectroscopy. Bioscience, Biotechnology, and Biochemistry **77**: 487–496.

747 **Pfeiffer, N., Tränkner, C., Lemnian, I., Grosse, I., Müller, A.E., Jung, C., and Kopisch-Obuch, F.J.** (2014).
748   Genetic analysis of bolting after winter in sugar beet (Beta vulgaris L.). Theoretical and applied
749   genetics **127**: 2479–2489.

750 **Pin, P.A. et al.** (2012). The Role of a Pseudo-Response Regulator Gene in Life Cycle Adaptation and
751   Domestication of Beet. Current Biology **22**: 1095–1101.

752 **Pin, P.A., Benlloch, R., Bonnet, D., Wremerth-Weich, E., Kraft, T., Gielen, J.J.L., and Nilsson, O.** (2010).
753   An Antagonistic Pair of *FT* Homologs Mediates the Control of Flowering Time in Sugar Beet.
754   Science **330**: 1397.

755 **Pommerrenig, B., Cvetkovic, J., Trentmann, O., Klemens, P.A.W., Neuhaus, H.E., and Ludewig, F.**
756   (2018). In Concert: Orchestrated Changes in Carbohydrate Homeostasis Are Critical for Plant
757   Abiotic Stress Tolerance. Plant and Cell Physiology **59**: 1290–1299.

758 **Ritz, C., Pipper, C., Yndgaard, F., Fredlund, K., and Steinrücken, G.** (2010). Modelling flowering of plants
759   using time-to-event methods. European Journal of Agronomy **32**: 155–161.

760 **Roitsch, T.** (1999). Source-sink regulation by sugar and stress. Current Opinion in Plant Biology **2**: 198–
761   206.

762 **Ronquist, F., Teslenko, M., van der Mark, P., Ayres, D.L., Darling, A., Höhna, S., Larget, B., Liu, L.,**
763   **Suchard, M.A., and Huelsenbeck, J.P.** (2012). MrBayes 3.2: Efficient Bayesian Phylogenetic
764   Inference and Model Choice Across a Large Model Space. Systematic Biology **61**: 539–542.

765 **Schneider, S., Hulpke, S., Schulz, A., Yaron, I., Höll, J., Imlau, A., Schmitt, B., Batz, S., Wolf, S., Hedrich,**
766   **R., and Sauer, N.** (2012). Vacuoles release sucrose via tonoplast-localised SUC4-type
767   transporters. Plant Biology **14**: 325–336.

768 **Schulz, A., Beyhl, D., Marten, I., Wormit, A., Neuhaus, E., Poschet, G., Büttner, M., Schneider, S., Sauer,**
769   **N., and Hedrich, R.** (2011). Proton-driven sucrose symport and antiport are provided by the
770   vacuolar transporters SUC4 and TMT1/2. The Plant Journal **68**: 129–136.

771 **Sievers, F., Wilm, A., Dineen, D., Gibson, T.J., Karplus, K., Li, W., Lopez, R., McWilliam, H., Remmert,**
772   **M., Söding, J., Thompson, J.D., and Higgins, D.G.** (2011). Fast, scalable generation of high-quality
773   protein multiple sequence alignments using Clustal Omega. Mol Syst Biol **7**: 539.

774 **Sonnewald, U. and Fernie, A.R.** (2018). Next-generation strategies for understanding and influencing
775   source–sink relations in crop plants. Current Opinion in Plant Biology **43**: 63–70.

776 **Srivastava, A.C., Ganesan, S., Ismail, I.O., and Ayre, B.G.** (2008). Functional Characterization of the
777   Arabidopsis AtSUC2 Sucrose/H$^+$ Symporter by Tissue-Specific Complementation Reveals an
778   Essential Role in Phloem Loading But Not in Long-Distance Transport. Plant Physiol. **148**: 200.

779 **Steponkus, P.L.** (1971). Cold Acclimation of *Hedera helix*. Plant Physiol. **47**: 175.

780 **Stitt, M., Lilley, R.McC., Gerhardt, R., and Heldt, H.W.** (1989). [32] Metabolite levels in specific cells and
781   subcellular compartments of plant leaves. In Methods in Enzymology (Academic Press), pp. 518–
782   552.

26

783 **Strand, Å., Hurry, V., Gustafsson, P., and Gardeström, P.** (1997). Development of Arabidopsis thaliana
784   leaves at low temperatures releases the suppression of photosynthesis and photosynthetic gene
785   expression despite the accumulation of soluble carbohydrates. The Plant Journal **12**: 605–614.

786 **Sturm, A.** (1996). Molecular characterization and functional analysis of sucrose-cleaving enzymes in
787   carrot (Daucus carota L.). Journal of Experimental Botany **47**: 1187–1192.

788 **Suzuki, N. and Mittler, R.** (2006). Reactive oxygen species and temperature stresses: a delicate balance
789   between signaling and destruction. Physiologia plantarum **126**: 45–51.

790 **Team, R.C.** (2017). R: A language and environment for statistical com-puting. R Foundation for Statistical
791   Computing, Vienna, Austria. URL https://www. R-project. org.

792 **Tränkner, C., Lemnian, I.M., Emrani, N., Pfeiffer, N., Tiwari, S.P., Kopisch-Obuch, F.J., Vogt, S.H., Müller,**
793   **A.E., Schilhabel, M., Jung, C., and Grosse, I.** (2016). A Detailed Analysis of the BR1 Locus
794   Suggests a New Mechanism for Bolting after Winter in Sugar Beet (Beta vulgaris L.). Frontiers in
795   Plant Science **7**: 1662.

796 **Tränkner, C., Pfeiffer, N., Kirchhoff, M., Kopisch-Obuch, F.J., van Dijk, H., Schilhabel, M., Hasler, M.,**
797   **and Emrani, N.** (2017). Deciphering the complex nature of bolting time regulation in Beta
798   vulgaris. Theoretical and Applied Genetics **130**: 1649–1667.

799 **Turesson, H., Andersson, M., Marttila, S., Thulin, I., and Hofvander, P.** (2014). Starch biosynthetic genes
800   and enzymes are expressed and active in the absence of starch accumulation in sugar beet tap-
801   root. BMC Plant Biology **14**: 104.

802 **Turgeon, R.** (1989). The sink-source transition in leaves. Annual review of plant biology **40**: 119–138.

803 **Viola, R., Pelloux, J., Van Der Ploeg, A., Gillespie, T., Marquis, N., Roberts, A.G., And Hancock, R.D.**
804   (2007). Symplastic connection is required for bud outgrowth following dormancy in potato
805   (Solanum tuberosum L.) tubers. Plant, Cell & Environment **30**: 973–983.

806 **Voll, H., Schießl, I., Hofmann, J., Volkert, K., Voll, L.M., Debast, S., Schneider, S., and Börnke, F.** (2014).
807   Loss of the two major leaf isoforms of sucrose-phosphate synthase in Arabidopsis thaliana limits
808   sucrose synthesis and nocturnal starch degradation but does not alter carbon partitioning during
809   photosynthesis. Journal of Experimental Botany **65**: 5217–5229.

810 **Whelan, S. and Goldman, N.** (2001). A general empirical model of protein evolution derived from
811   multiple protein families using a maximum-likelihood approach. Molecular biology and evolution
812   **18**: 691–699.

813 **Wingenter, K., Schulz, A., Wormit, A., Wic, S., Trentmann, O., Hoermiller, I.I., Heyer, A.G., Marten, I.,**
814   **Hedrich, R., and Neuhaus, H.E.** (2010). Increased Activity of the Vacuolar Monosaccharide
815   Transporter TMT1 Alters Cellular Sugar Partitioning, Sugar Signaling, and Seed Yield in
816   Arabidopsis. Plant Physiol. **154**: 665.

817 **Wolfe, J. and Bryant, G.** (1999). Freezing, Drying, and/or Vitrification of Membrane– Solute–Water
818   Systems. Cryobiology **39**: 103–129.

819

820

821 **Figure legends**

822 **Figure 1.** Biomass and sugar accumulation response to cold temperatures in shoots and taproots of 6-week old sugar

823 beet plants from three different genotypes (GT1 = grey square; GT2 = blue circle; GT3 = brown triangle). Plants were

824 grown for six weeks at 20°C, then transferred to 12°C for one week and then to 4°C (start of recording of biomass and

825 sugar accumulation) for 19 days. For each data point, whole organs (shoots or taproots) were harvested at midday.

826 Data points show means from n=6 to 10 plants ± SD. **(A, B)** Fresh weight (FW), dry weight (DW) and water content

827 of shoots and roots. **(C, D)** Sugar and starch accumulation during the course of the chilling (4°C) period in shoots and

828 taproots, respectively. Significant changes to the control condition (first data point) were calculated using double sided

829 Student's *t*-test (* = $p < 0.05$).

830

831 **Figure 2.** Photosynthetic parameters, CO_2 assimilation, and expression data of sugar beet leaves after cold exposure.

832 Sugar beet plants of three genotypes (GT1 = grey square; GT2 = blue circle; GT3 = brown triangle) were grown for

833 six weeks at 20°C and then transferred to 12°C for one week and then to 4°C for three weeks. **(A)** PAM measurements

834 of leaves of the three different genotypes. Quantum yield of photosynthesis [Y(II)], of non-photochemical quenching

835 [Y(NPQ)], and of non-regulated quenching [Y(NO)]. At each time point four plants per genotype were analyzed. **(B)**

836 Gas exchange measured for the same plants as used in **A)**. Intercellular leaf CO_2 concentration (C_i), CO_2 assimilation

837 rate (*A*), and transpiration rate (*E*) are depicted. For each measurement, four independent plants were used. The very

838 same plants were used for the measurements at the different time points after transfer to cold conditions. Significant

839 changes to the control condition (first data point) were calculated using Student's *t*-test (* = p < 0.05). **(C)** Principal

840 component analysis (PC1 *versus* PC2) for three genotypes based on expression values of 162 photosynthesis-related

841 genes extracted from RNA-seq data of source leaves from plants grown at 20°C after exposure to 4°C or to control

842 conditions (20°C) for 14 days, respectively. **(D)** Percentage of RNA-Seq reads annotated as genes coding for

843 photosynthesis (PS) related proteins. Pie charts represent the averaged means from three different genotypes at 20°C

844 (control) and after 14 days at 4°C. **(D)** Expression of *RubisCO Activase* (*Bv2_025300_tzou.t1*), *RubisCO small subunit*

845 (*Bv2026840_jycs_t1*), *Chlorophyll A/B binding protein A* (*Bv_002570_dmif.t1*, *Plastocyanin* (*Bv_004160_hgjn.t1*),

846 *Glutathione reductase1* (*Bv3_069540_erom.t1*), *Glutathione reductase2* (*Bv5_120360_jpwm.t1*), *Superoxide*

847 *dismutase1* (*Bv5_102420_sxsu.t1*), *Ascorbate peroxidase1* (*Bv1_007470_ymzt.t1*). Data represent the mean

848 normalized cpm values of three independent RNA-seq analyses per genotype and temperature condition ± SD.

849 Asterisks represent *p*-values < 0.05 according to double sided *t*-test in comparison to the values at control condition

850 (20°C).

851

852 **Figure 3.** Changes in major carbohydrate metabolism and energy state in response to cold. **(A)** Respiration (CO_2

853 production) of different taproot regions from GT1 under control conditions (20°C, yellow bars) or after one week

854 transfer to 4°C (blue bars). **(B)** Respiration (CO_2 production) from leaf tissue of three genotypes (GT1, GT2, GT3)

855 under control conditions (20°C, yellow bars) or after 1-week transfer to 4°C (blue bars). **(C)** Principal component (PC)

856 analysis (PC1 *versus* PC2) for three genotypes based on expression values of 112 genes with GO annotation "major

857 CHO metabolism" (loadings) extracted from RNA-seq data of source leaves from plants grown at 20°C and transferred

28

858   for 1 week at 12°C followed by 14 days at 4°C or control conditions (20°C). **(D)** Heatmap analysis of grouped

859   expression values extracted from RNA-seq data. Unit variance scaling was applied to rows. Rows are clustered using

860   Manhattan distance and average linkage. **(E)** Expression values for two Sucrose Phosphate Synthase genes (*BvSPSA1*

861   and *BvSPSA2*) extracted from RNA-seq data of shoots and roots and expression values for two Sucrose Synthase genes

862   (*BvSUS1* and *BvSUS2*) extracted from RNA-seq data of shoots and roots from GT1, GT2, GT3. Data represent the

863   mean normalized cpm values of three independent RNA-seq analyses per genotype and temperature condition ± SD.

864   **(F)** ATP, ATP/ADP ratio, energy charge, EC = [ATP] + 0.5 [ADP]/[ATP] + [ADP] + [AMP]. **(E/F)** Data are means

865   ± SD. Asterisks represent *p*-values < 0.05 according to double sided *t*-test in comparison to the values at control

866   condition (20°C).

867

868   **Figure 4.** Distribution of ^{14}C-sucrose and esculin in leaves. **(A-D)** Autoradiography of ^{14}C-sucrose in leaves. **(A)**

869   Schematic depiction of experiment. Taproots were inoculated with ^{14}C-sucrose solution and harvested and dried leaves

870   were autoradiographed one week later. **(B)** Source leaf from a representative plant grown for one week under at 4°C.

871   Blackening of veins indicates radioactivity incorporated and distributed into leaf tissue after injection of radiolabeled

872   sucrose into taproots. Abbreviations: p = petiole; mv = middle vein; 1° = first order lateral vein; 2° = second order

873   lateral vein. **(C)** Source leaf from representative control plant grown at 20°C. **(D)** radioactivity in cpm (counts per

874   minute) measured in isolated petioles from plants grown under 4 or 20°C. Center lines show the medians; box limits

875   indicate the 25th and 75th percentiles; whiskers extend 1.5 times the interquartile range from the 25th and 75th

876   percentiles, outliers are represented by dots; crosses represent sample means; n = 16 sample points. **(E-K)** Esculin

877   loadings. Yellow fluorescence indicates lignified xylem vessels, blue fluorescence indicates esculin trafficking. **(E)**

878   Schematic depiction of experiment. Esculin was loaded onto the scratched surface of a source leaf of plants grown at

879   20°C. Loaded plants were transferred to 4°C or kept at 20°C. Petioles of neighbored, not loaded source leaves were

880   analyzed for esculin fluorescence in plants from 4°C or 20°C. **(F-I)** Cross sections through petiole of a source leaf not

881   loaded with esculin from plants loaded at 20°C. **(F, G)** Petioles from 20°C **(F)** Bright field image. **(G)** UV fluorescence

882   image. **(H, I):** Petioles from 4°C. **(H)** Bright field image. **(I)** UV fluorescence image. **(J, K)** Longitudinal sections of

883   a petiole from 4°C. **J)** Bright field image. **K)** UV fluorescence image. Abbreviations: xy: xylem, ph: phloem. Bars are

884   50µm in G and H and 100µm in E, F, I, and J.
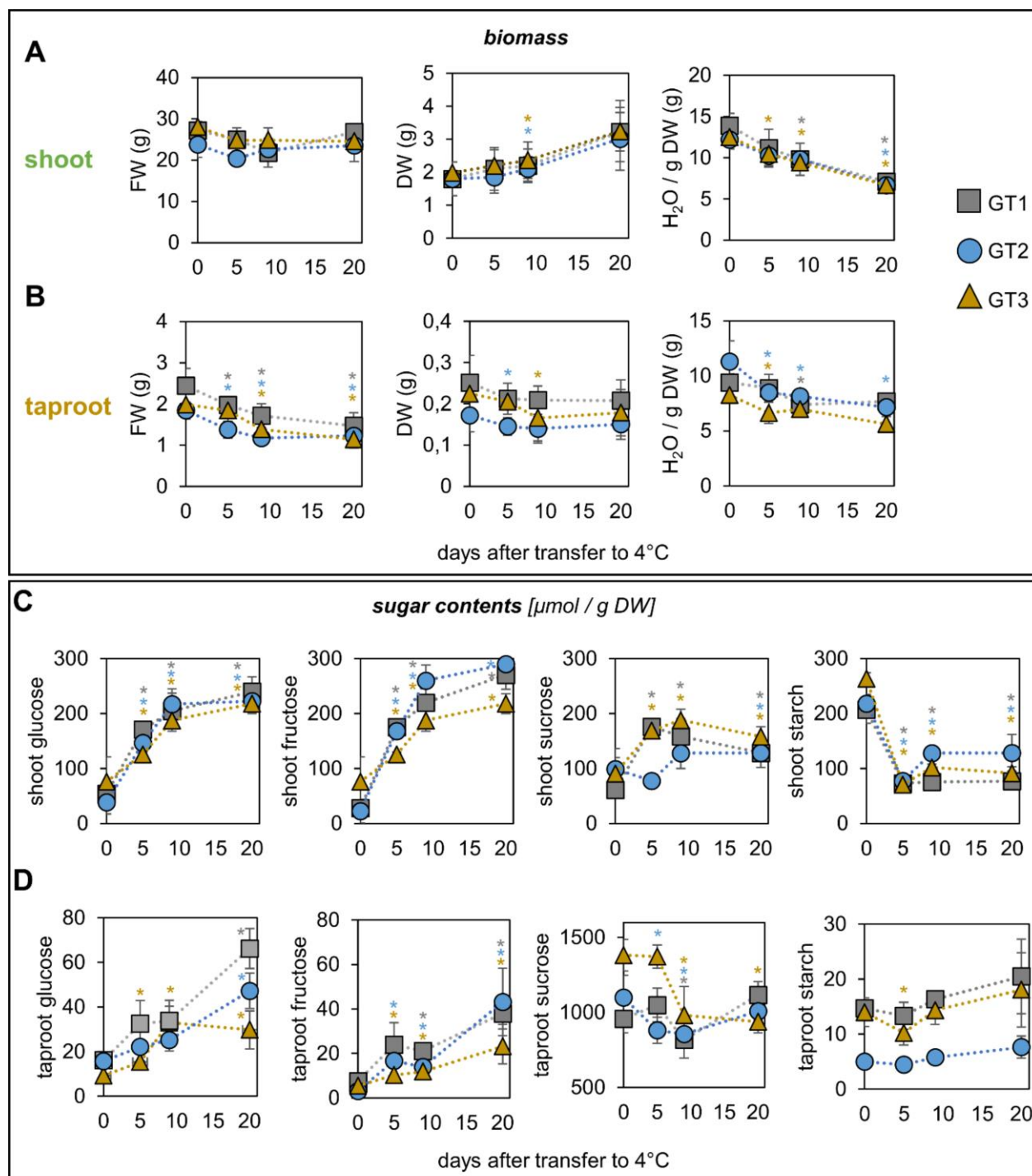
885

886   **Figure 5.** Cold-dependent accumulation of *BvTST2;1* and *BvSUT4* in three different sugar beet genotypes. **(A)**

887   Illustration on cold-induced processes. Upper image: Cold-dependent sugar relocations from taproots to shoots. Middle

888   image: schematic of taproot vacuolar transport processes and factors. Vacuolar ATPase (V-H$^+$-ATPase) establishes a

889   proton motif force (pmf) across the vacuolar membrane; TST2;1 acts as proton/sucrose antiporter using pmf for sucrose

890   import into vacuoles. SUT4 acts as proton/sucrose symporter using pmf for vacuolar sucrose export. Bottom image:

891   reciprocal cold-induced regulation of BvTST2;1 and BvSUT4 mRNA levels in taproots **(B)** Transcript abundance of

892   BvTST2;1 (Bv5_115690_zuju) mRNA based on RNA-seq reads. Values represent means from n=3 biological

893   replicates per genotype ± SE. **(C)** Transcript abundance of BvSUT4 (Bv5_124860_zpft.t1) mRNA based on RNA-seq

894   reads. Values represent means from n=3 (mRNA) biological replicates ± SE. Asterisks indicate significant differences

895   between the 20°C and 4°C treatments according to t-test (* = p < 0.05). **(D)** Subcellular localisation of BvSUT4-GFP

896   in Arabidopsis or *Beta vulgaris* leaf mesophyll protoplasts. Single optical sections in all pictures. The green colour

897   shows the GFP-signal; the chlorophyll auto fluorescence is shown in red. Bars = 5 μm. Arrowheads point towards the

898   vacuolar membrane (tonoplast).

899

900   **Figure 6.** Expression of floral regulator genes. Transcript abundances of *BvBBX19* (Bv9_216430_rwmw.t1), *BvBTC1*

901   (Bv2_045920_gycn.t1), *BvFT1* (Bv9_214250_miuf.t1), and *BvFT2* (Bv4_074700_eewx.t1) based on RNA-seq reads

902   in shoots and taproots of three different genotypes. Values represent means from n=3 biological replicates ± SE.

903   Asterisks indicate *p*-values < 0.05 according to double sided *t*-test.
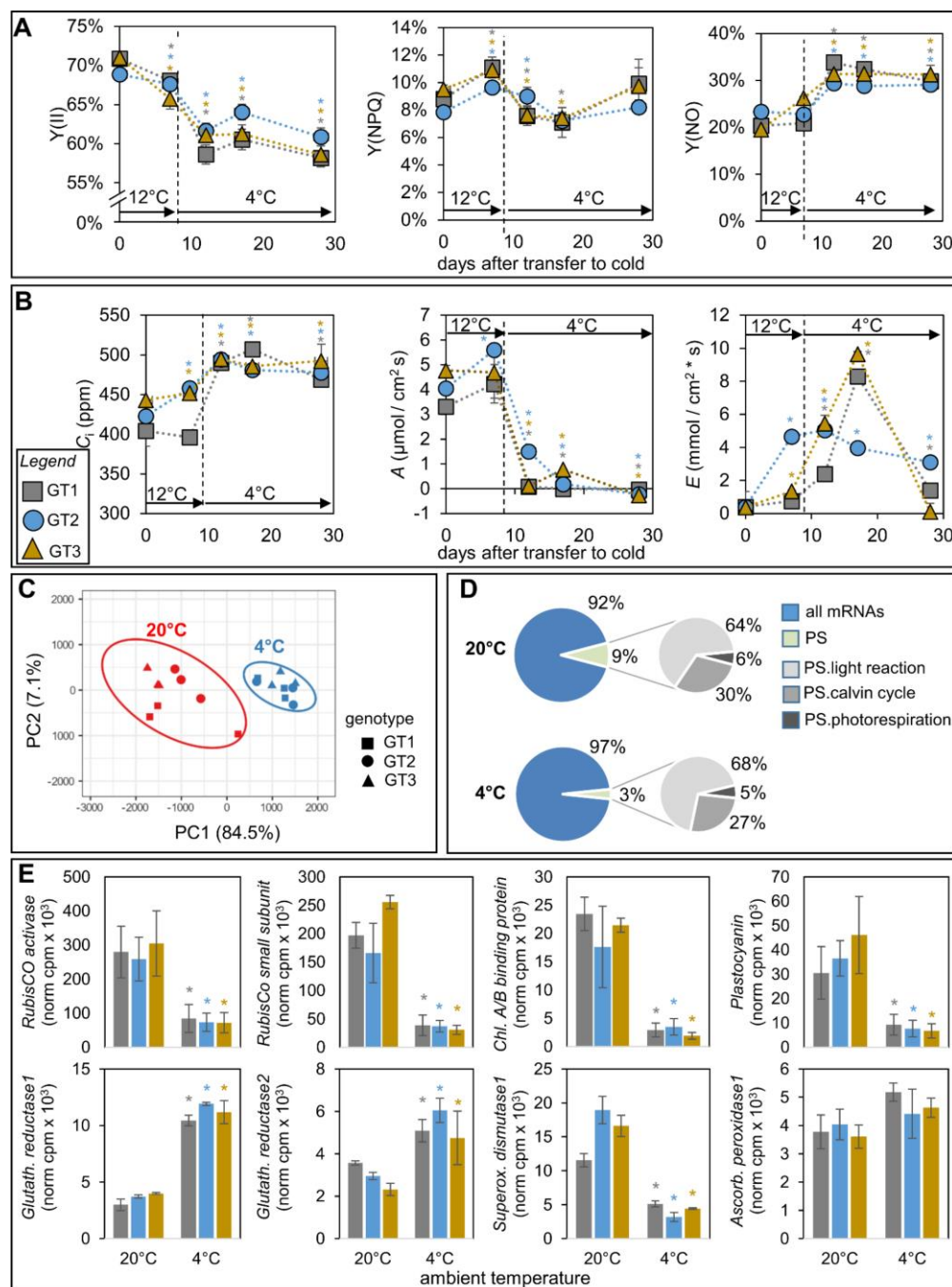
904   **Figure 7.** Schematic illustration of cold-induced sink to source transition. Leaf- and taproot-tissue of sugar beet are

905   reprogrammed and source and sink identities shifted upon cold. Shoots adopt sink identity during cold. Biomass and

906   sugar concentration in the shoot increase **(A)** despite reduced photosynthetic activity and inactivation of carbon

907   assimilation **(B)**. Concomitantly, shoot respiration increases **(C)** and cellular starch pools decrease **(D)**. Contrastingly,

908   taproots show a decrease of sucrose levels **(E)** but lower respiration rate **(F)** as well as increased sucrose biosynthesis

909   **(G)**. Taproot sugar is remobilized in the cold due to opposite regulation of taproot-specific vacuolar sucrose importer

910   (BvTST2;1) and exporter (BvSUT4) activity **(H)**. Taken together, this results in a reversal of the phloem translocation

911   stream **(I)** triggered by a reprogramming of source and sink identities, which might correlate with inflorescence

912   initiation.

913

Figure 1. Biomass and sugar contents in the cold.
Response to cold temperatures of shoots and taproots of 6-week old sugar beet plants from three different genotypes (GT1 = grey square; GT2 = blue circle; GT3 = brown triangle). Plants were grown for six weeks at 20°C, then transferred to 12°C for one week and then to 4°C (start of recording of biomass and sugar accumulation) for 19 days. For each data point, whole organs (shoots or taproots) were harvested at midday. Data points show means from n=6 to 10 plants ± SD. **(A, B)** Fresh weight (FW), dry weight (DW) and water content of shoots and roots. **(C, D)** Sugar and starch accumulation during the course of the chilling (4°C) period in shoots and taproots, respectively. Significant changes to the control condition (first data point) were calculated using double sided Student's t-test (* = $p < 0.05$).

914

915

31

Figure 2. Photosynthetic parameters, CO₂ assimilation and expression data of sugar beet leaves after cold exposure.
Sugar beet plants of three genotypes (GT1 = grey square; GT2 = blue circle; GT3 = brown triangle) were grown for six weeks at 20°C and then transferred to 12°C for one week and then to 4°C for three weeks. **(A)** PAM measurements of leaves of the three different genotypes. Quantum yield of photosynthesis [Y(II)], of non-photochemical quenching [Y(NPQ)], and of non-regulated quenching [Y(NO)]. At each time point four plants per genotype were analyzed. **(B)** Gas exchange measured for the same plants as used in **(A)**. Intercellular leaf CO₂ concentration (C_i), CO₂ assimilation rate (*A*), and transpiration rate (*E*) are depicted. For each measurement, four independent plants were used. The very same plants were used for the measurements at the different time points after transfer to cold conditions. Significant changes to the control condition (first data point) were calculated using Student's *t*-test (* = p < 0.05). **(C)** Principal component analysis (PC1 *versus* PC2) for three genotypes based on expression values of 162 photosynthesis-related genes extracted from RNA-seq data of source leaves from plants grown at 20°C after exposure to 4°C or to control conditions (20°C) for 14 days, respectively. **(D)** Percentage of RNA-Seq reads annotated as genes coding for photosynthesis (PS) related proteins. Pie charts represent the averaged means from three different genotypes at 20°C (control) and after 14 days at 4°C. **(D)** Expression of *RubisCO Activase* (*Bv2_025300_tzou.t1*), *RubisCO small subunit* (*Bv2026840_jycs_t1*), *Chlorophyll A/B binding protein A* (*Bv_002570_dmif.t1*, *Plastocyanin* (*Bv_004160_hgjn.t1*), *Glutathione reductase1* (*Bv3_069540_erom.t1*), *Glutathione reductase2* (*Bv5_120360_jpwm.t1*), *Superoxide dismutase1* (*Bv5_102420_sxsu.t1*), *Ascorbate peroxidase1* (*Bv1_007470_ymzt.t1*). Data represent the mean normalized cpm values of three independent RNA-seq analyses per genotype and temperature condition ± SD. Asterisks represent *p*-values < 0.05 according to double sided *t*-test in comparison to the values at control condition (20°C).

916
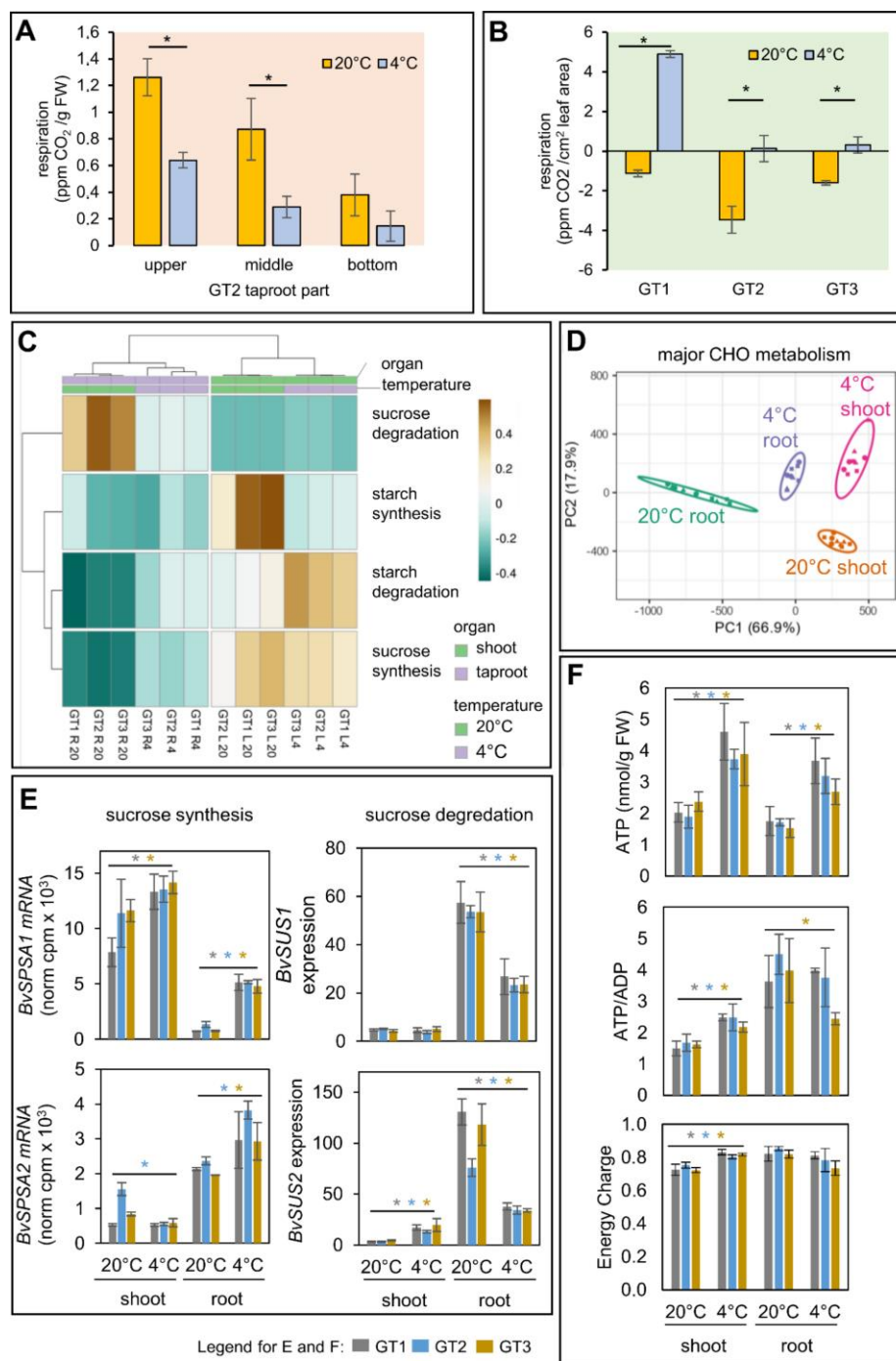
Figure 3. Changes in major carbohydrate metabolism and energy state in response to cold.
(A) Respiration (CO_2 production) of different taproot regions from GT1 under control conditions (20°C, yellow bars) or after one week transfer to 4°C (blue bars). **(B)** Respiration (CO_2 production) from leaf tissue of three genotypes (GT1, GT2, GT3) under control conditions (20°C, yellow bars) or after 1-week transfer to 4°C (blue bars). **(C)** Principal component (PC) analysis (PC1 *versus* PC2) for three genotypes based on expression values of 112 genes with GO annotation "major CHO metabolism" (loadings) extracted from RNA-seq data of source leaves from plants grown at 20°C and transferred for 1 week at 12°C followed by 14 days at 4°C or control conditions (20°C). **(D)** Heatmap analysis of grouped expression values extracted from RNA-seq data. Unit variance scaling was applied to rows. Rows are using Manhattan distance and average linkage. **(E)** Expression values for two Sucrose Phosphate Synthase genes (*BvSPSA1* and *BvSPSA2*) and for two Sucrose Synthase genes (*BvSUS1* and *BvSUS2*) extracted from RNA-seq data of shoots and roots from GT1, GT2, GT3. Data represent the mean normalized cpm values of three independent RNA-seq analyses per genotype and temperature condition ± SD. **(F)** ATP, ATP/ADP ratio, energy charge, EC = [ATP] + 0.5 [ADP]/[ATP] + [ADP] + [AMP]. **(E,F)** Data are means ± SD. Asterisks represent *p*-values < 0.05 according to double sided *t*-test in comparison to the values at control condition (20°C).

917
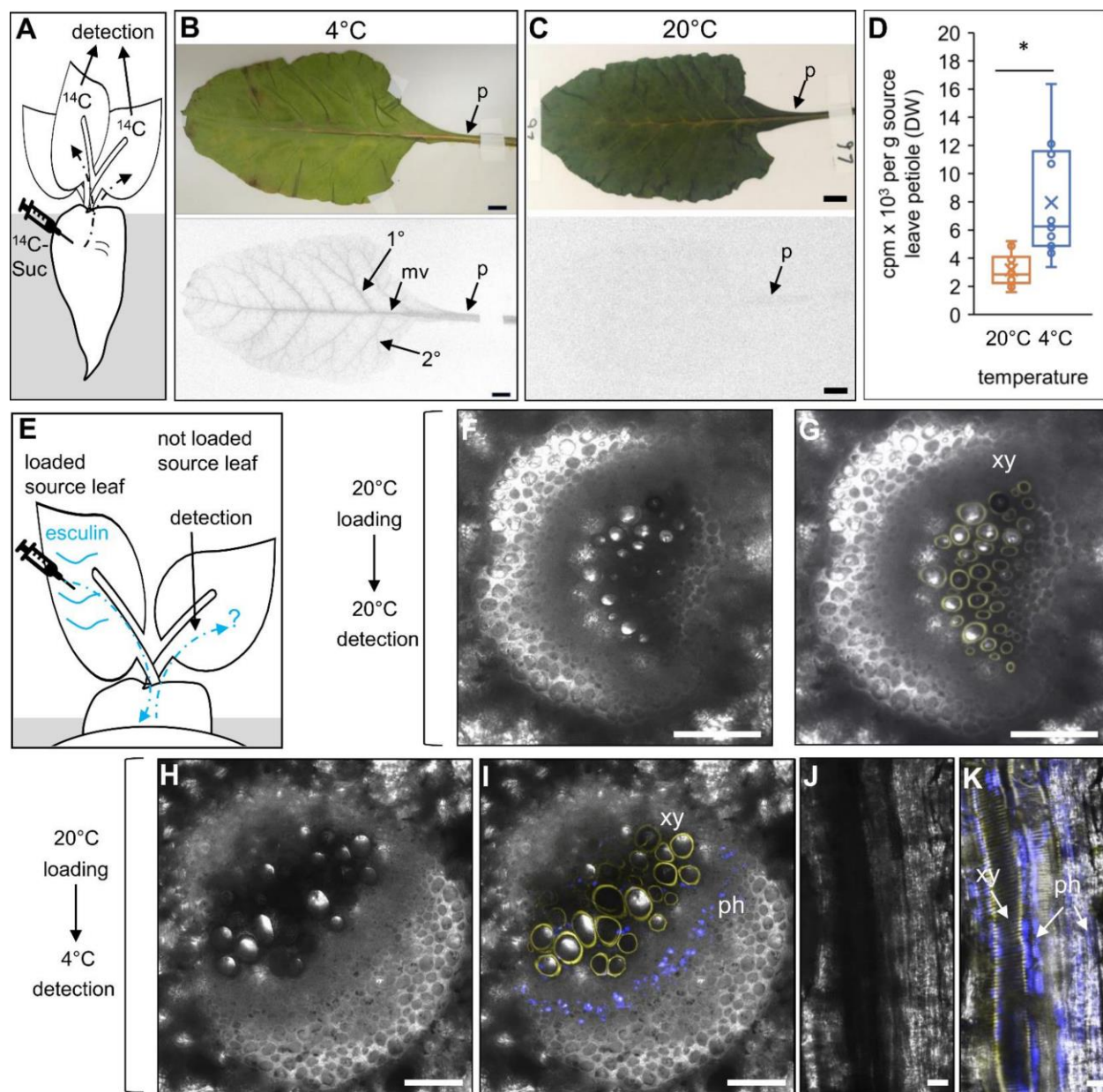
Figure 4. Distribution of ^{14}C-sucrose and esculin in leaves.

(A-D) Autoradiography of ^{14}C-sucrose in leaves. **(A)** Schematic depiction of experiment. Taproots were inoculated with ^{14}C-sucrose solution and harvested and dried leaves were autoradiographed one week later. **(B)** Source leaf from a representative plant grown for one week under at 4°C. Blackening of veins indicates radioactivity incorporated and distributed into leaf tissue after injection of radiolabeled sucrose into taproots. Abbreviations: p = petiole; mv = middle vein; 1° = first order lateral vein; 2° = second order lateral vein. **(C)** Source leaf from representative control plant grown at 20°C. **(D)** Radioactivity in cpm (counts per minute) measured in isolated petioles from plants grown under 4 or 20°C. Center lines show the medians; box limits indicate the 25th and 75th percentiles; whiskers extend 1.5 times the interquartile range from the 25th and 75th percentiles, outliers are represented by dots; crosses represent sample means; n = 16 sample points. **(E-K)** Esculin loadings. Yellow fluorescence indicates lignified xylem vessels, blue fluorescence indicates esculin trafficking. **(E)** Schematic depiction of experiment. Esculin was loaded onto the scratched surface of a source leaf of plants grown at 20°C. Loaded plants were transferred to 4°C or kept at 20°C. Petioles of neighbored, not loaded source leaves were analyzed for esculin fluorescence in plants from 4°C or 20°C. **(F-K)** Sections through a petiole of a source leaf not loaded with esculin. **(F,G)** Cross sections of petioles from 20°C **(F)** Bright field image. **(G)** UV fluorescence image. **(H, I)** Petioles from 4°C. **(H)** Bright field image. **(I)** UV fluorescence image. **(J, K)** Longitudinal sections of a petiole from 4°C. **J)** Bright field image. **K)** UV fluorescence image. Abbreviations: xy: xylem, ph: phloem. Bars are 100µm in **F-I** and 100µm in **J** and **K**.
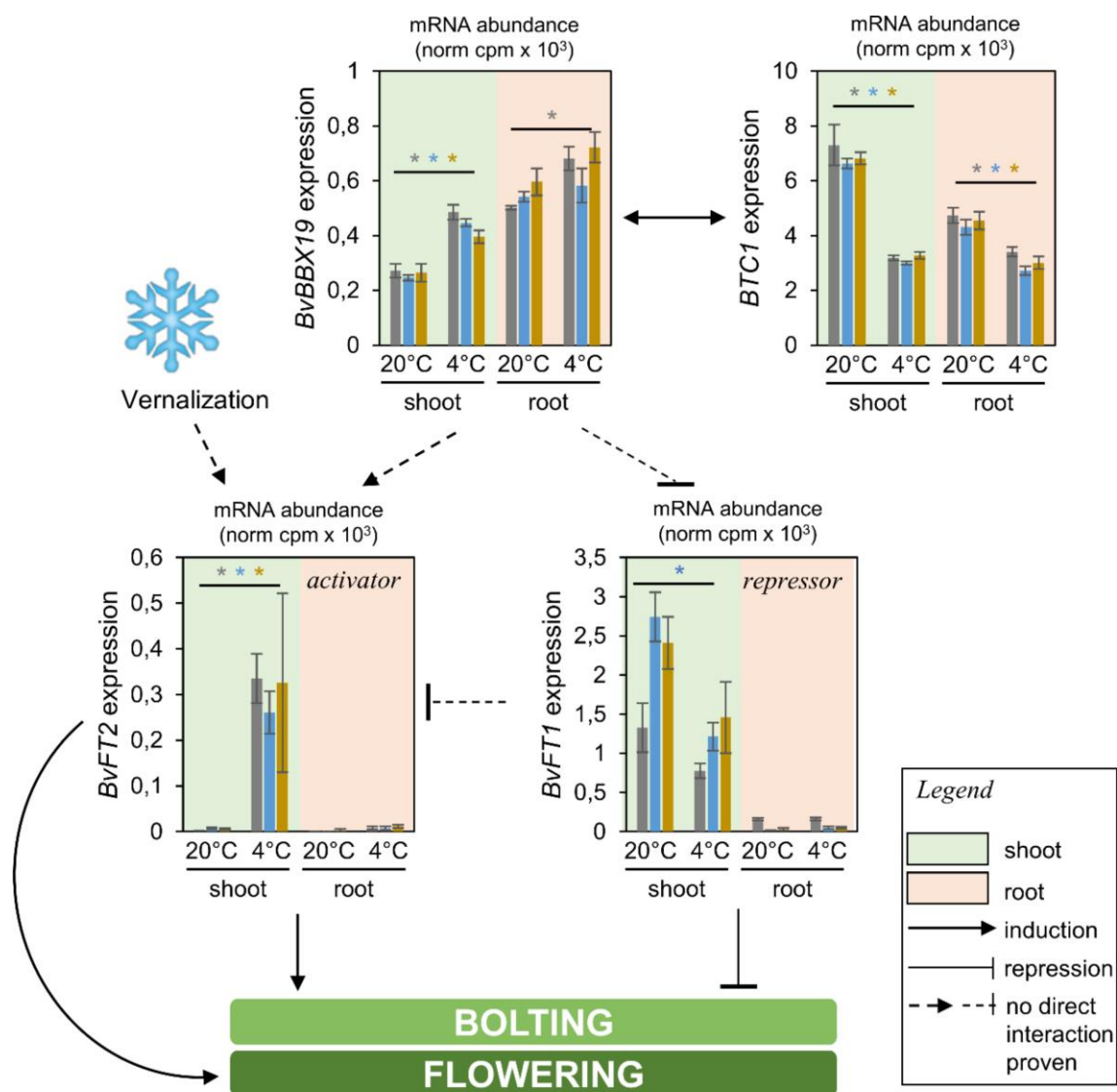
918

919
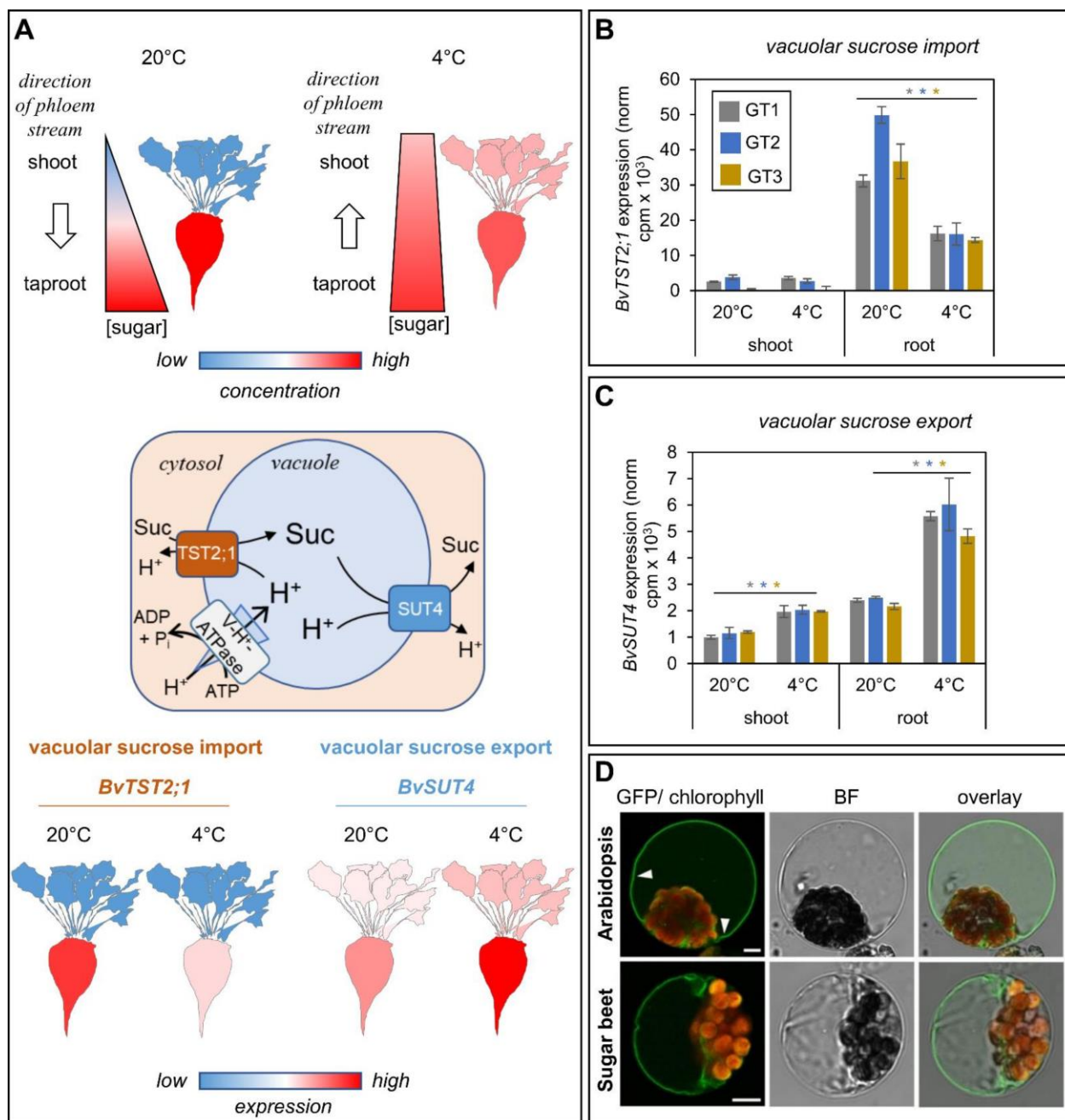
Figure 5. Cold-dependent accumulation of *BvTST2;1* and *BvSUT4* in three different sugar beet genotypes.
(A) Illustration on cold-induced processes. Upper image: Cold-dependent sugar relocations from taproots to shoots. Middle image: schematic of taproot vacuolar transport processes and factors. Vacuolar ATPase (V-H$^+$-ATPase) establishes a proton motif force (pmf) across the vacuolar membrane; TST2;1 acts as proton/sucrose antiporter using pmf for sucrose import into vacuoles. SUT4 acts as proton/sucrose symporter using pmf for vacuolar sucrose export. Bottom image: reciprocal cold-induced regulation of BvTST2;1 and BvSUT4 mRNA levels in taproots. **(B)** Transcript abundance of *BvTST2;1* (Bv5_115690_zuju) mRNA based on RNA-seq reads. Values represent means from n=3 biological replicates per genotype ± SE. **(C)** Transcript abundance of *BvSUT4* (Bv5_124860_zpft.t1) mRNA based on RNA-seq reads. Values represent means from n=3 (mRNA) biological replicates ± SE. Asterisks indicate significant differences between the 20°C and 4°C treatments according to t-test (* = $p < 0.05$). **(D)** Subcellular localisation of BvSUT4-GFP in Arabidopsis or *Beta vulgaris* leaf mesophyll protoplasts. Single optical sections in all pictures. The green colour shows the GFP-signal, the chlorophyll auto fluorescence is shown in red. Bars = 5 μm. Arrowheads point towards the vacuolar membrane (tonoplast).
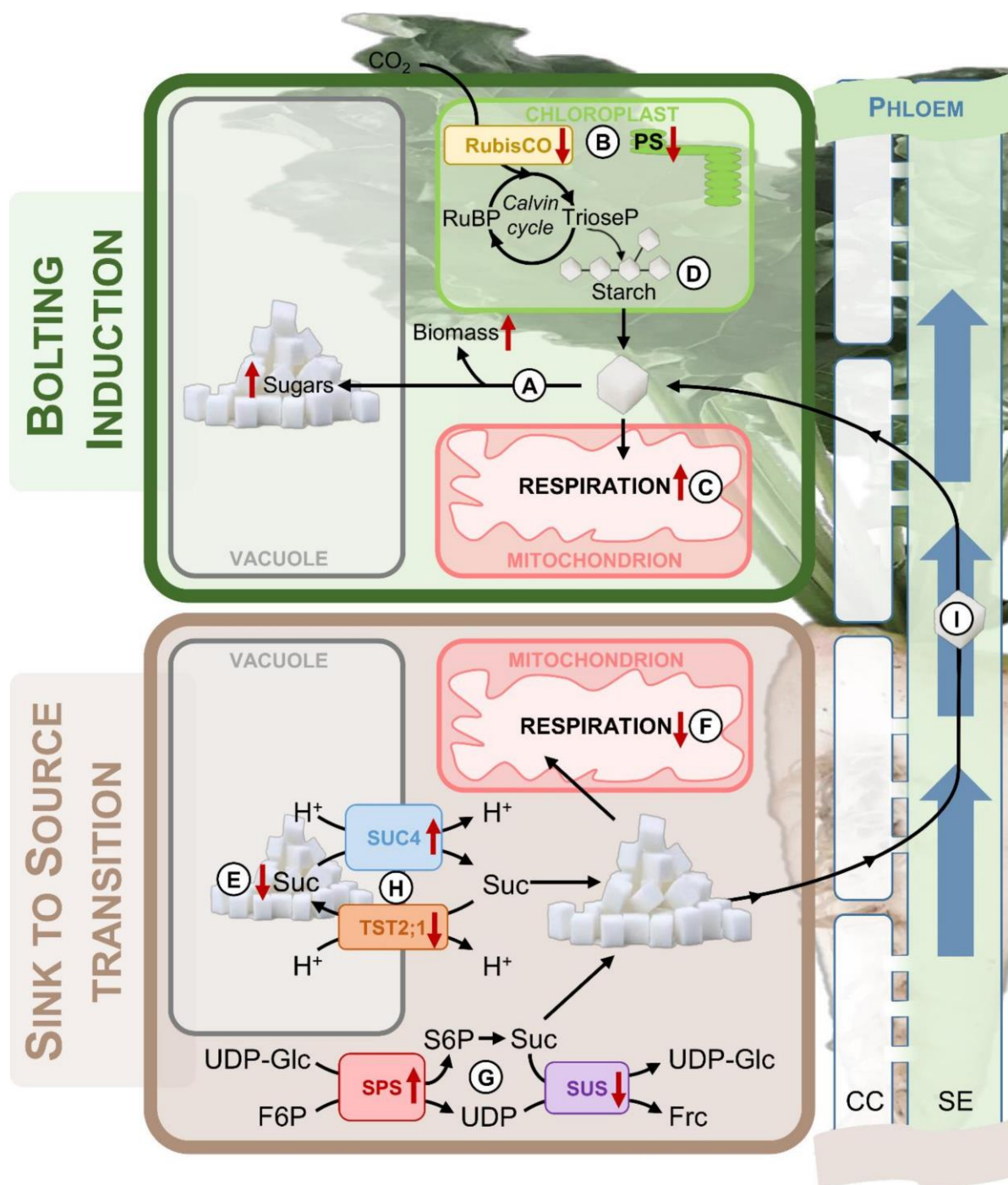
920

921

Figure 6. Expression of floral regulator genes.
Transcript abundances of *BvBBX19* (Bv9_216430_rwmw.t1), *BvBTC1* (Bv2_045920_gycn.t1), *BvFT1* (Bv9_214250_miuf.t1), and *BvFT2* (Bv4_074700_eewx.t1) based on RNA-seq reads in shoots and taproots of three different genotypes. Values represent means from n=3 biological replicates ± SE. Asterisks indicate *p*-values < 0.05 according to double sided *t*-test.

922

923

Figure 7. Schematic illustration of cold-induced sink to source transition.

Leaf- and taproot-tissue of sugar beet are reprogrammed and source and sink identities shifted upon cold. Shoots adopt sink identity during cold. Biomass and sugar concentration in the shoot increase **(A)** despite reduced photosynthetic activity and inactivation of carbon assimilation **(B)**. Concomitantly, shoot respiration increases **(C)** and cellular starch pools decrease **(D)**. Contrastingly, taproots show a decrease of sucrose levels **(E)** but lower respiration rate **(F)** as well as increased sucrose biosynthesis **(G)**. Taproot sugar is remobilized in the cold due to opposite regulation of taproot-specific vacuolar sucrose importer (BvTST2;1) and exporter (BvSUT4) activity **(H)**. Taken together, this results in a reversal of the phloem translocation stream **(I)** triggered by a reprogramming of source and sink identities, which might correlate with inflorescence initiation.

924

37